ABSTRACT

Title of Thesis: LARGE AREA ALL-ELASTOMER
                    TACTILE SENSORS FOR ROBOTIC SKINS

                    Peter Block, Master of Science, 2014

Directed by: Professor Sarah Bergbreiter
                    Department Mechanical Engineering and
                    The Institute for Systems Research

This work demonstrates the first low cost, all-elastomer capacitive tactile arrays compatible with roll-to-roll manufacturing. A new manufacturing process has been developed in which elastomer sheets are covered with a stencil, spray coated with conductive elastomer on one or both sides, and stacked to create the sensor array. These arrays are highly flexible and can withstand large strains. Sensor costs are below $0.12/sensor in small quantities. Some variants in the fabrication process result in a slightly curved sensor so the change in capacitance is highly nonlinear at low pressures, but approaches theoretical sensitivities at higher pressures. The sensors have been determined to be highly sensitive, with a sensor resolution of 0.5 Pa and reveal a repeatable response from 1 kPa up to 120 kPa. A variety of materials ranging in modulus, thickness and texture were investigated for static, dynamic, and spatial location testing.

LARGE AREA ALL-ELASTOMER
TACTILE SENSORS FOR ROBOTIC SKINS

by

Peter Block

Thesis submitted to the Faculty of the Graduate School of the
University of Maryland, College Park in partial fulfillment
of the requirements for the degree of
Master of Science
2014

Advisory Committee:
Professor Sarah Bergbreiter, Chair/Advisor
Professor Pamela Abshire
Professor Elisabeth Smela

Dedication

To my fiancée, family and friends for their love and support they have provided throughout the years, to those dedicated to a lifetime of learning and to the giants whose shoulders we stand upon.

Acknowledgments

I would like to thank my advisor, Professor Sarah Bergbreiter, for the honor and privlege to conduct research in the MicroRobotics Laboratory. Her advice and insight on research, course work, and life has been invaluable to me. I wish all the best for her family and research work.

I would like to thank Professor Elisabeth Smela and Professor Pamela Abshire for their guidance, critique and advice in developing my thesis and serving on my examination committee.

I would like to thank the now graduated Dr. Aaron Garrett, for his aid and advice in developing this project. I would also like to thank the graduate students Alexi Charlambides, Dana Vogtmann, Abraham Simpson Chen, and Ivan Penskiy. Firstly, Alexi Charlambides for the static test design setup. This simple yet effective design has been cruicial to my data collection, so many thanks! I want to also thank graduate Dana Vogtmann for all the time provided for working with the laser cutter, and thanks to her, Alexi and Simpson for advice and critique of my presentations and thesis. I would also like to thank graduate student Ivan Penskiy for his advice in printed circuit board development and soldering techniques, and undergraduate Daniel Mirsky, thank you for your aid in better understanding the underlying theories, fabrication and programming of microelectronics.

I would lastly like to thank my folks for supporting me all these years, and fiancée, Lisa, for putting up with my long nights at the lab and your unconditional love.

Table of Contents

List of Tables

List of Figures

List of Abbreviations

SI	International System of Units
ω	Ohm, SI unit of measurement for resistance
F	Farad, SI unit of measurement for capacitance
N	SI unit of measurement for force, weight
Pa	SI unit of measurement for pressure, stress
m	SI unit of measurement for distance
μm	micrometer
AD	Analog Devices, a semiconductor company
ASP	Amazon Small Parts, a materials and equipment company
Cap.	Capacitance
CB	Carbon Black, a fine powder
COTS	Commercial off-the-shelf
CNT	Carbon Nanotubes, may be Single Walled SW or MultiWalled MW
cPDMS	Conductive PDMS
DARPA	Defense Advanced Research Projects Agency
Matl.	Material
Mfr.	Manufacturer
MMC	McMaster Carr, a materials and equipment company
PCB	Printed Circuit Board
Pkg.	Package
PU	Polyurethane
PDMS	Polydimethylsiloxane
Rez.	Resolution
SL	Silicon Labs, a semiconductor company
SW	Software
Viz.	Visualization

Chapter 1:   Introduction

As society moves towards increased automation and interaction with robotics, it will be essential that the robots will not only be able to communicate with the world via vision and locomotion, but also be able to touch and feel the world as well, especially when collaborating with humans or requiring extra dexterity in manipulating objects. Human robot interaction environments are increasingly becoming more prevalent and robotics systems are expected to be adaptive and reactive to new environments (DARPA robotics challenge 2013), while prosthetics continue improving greatly in functionality and mobility. Thus it will be necessary that there are sensing systems that provide robots and prosthetics users not only the capability of sensing the world around them, but the ability to manipulate and interact with it as well. Some possible scenarios may be an elderly home-care utilizing robots such as Asimo and the Ri-Man Robot (Figures 1.1a & 1.1b) , recovering the lost functionality of a missing body appendage with a Shadow hand (Figure 1.1c), or teleoperating the Robonaut (Figure 1.1d) for sampling planetary geology. Thus by considering tactile sensation we can help robots and prosthetic systems identify if a human hand or object is on a body part or be able to provide the tactile feedback to know the pressure needed to grip and change a light bulb, or the delicate forces

needed to pick up and safely secure an elderly person.
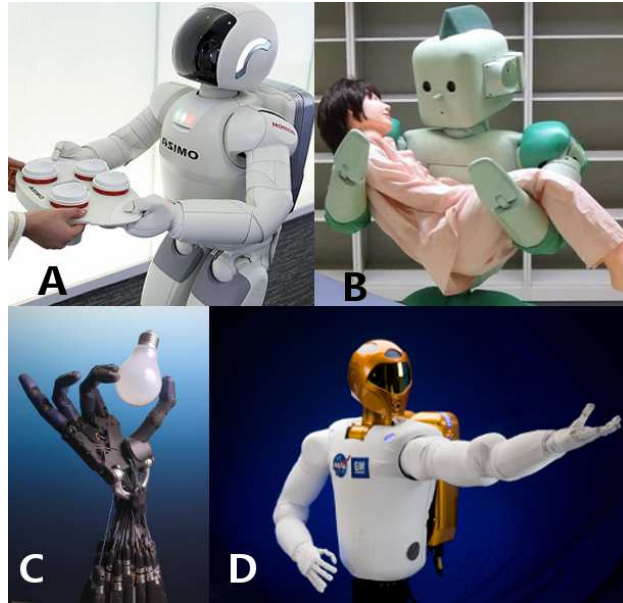
Figure 1.1: Various robots requiring sensing systems

Tactile sensors have been an area looked at for more than 30 years, and extensive reviews of the advancements have been identified throughout the decades [8, 9, 10]. To match human touch and sensing capabilities, it is important that materials are conformal and the sensors are capable of measuring forces that human skin can detect. Yet even elastomer tactile sensors such as silver doped rubber and carbon fiber mats had been listed as "current developments" since the 1980's [11]. Previous work includes a variety of flexible substrates such as polymer foams [6]) , films [2, 12, 13] , and elastomer channels [14]. Tactile transduction methods have also been studied by working with different properties like resistance [14, 15] , capacitance [16, 17, 18, 19] , or piezoelectricity [20, 21] to measure forces. Yet much of this work suffers from temperature dependence, hysteresis, and the lack of low

power electronics.

Of these transduction methods, capacitance enables high sensitivity and is able to provide high spatial resolution while sensing is independent of temperature change [10]. Utilizing capacitance as a means of sensing has also long been utilized, dating back to the 1960's and likely back even further [22]. But thanks to the ubiquity of capacitive devices in society today, such as cell phone touch screens, low power and relatively inexpensive capacitive sensing electronics are widely available for use in tactile sensing.

Elastomer capacitive tactile arrays as a subject alone has been investigated extensively [23, 16, 18, 17, 19] . Mannsfeld et al. utilized indium tin oxide and polyethylene with polydimethylsiloxane (PDMS) microstructures to create capacitors which were capable of measuring pressures as low as 5 Pa, though an array of these capacitors was not integrated into a system [19]. Instead a separate system of capacitance based organic field effect transistors was created by exploiting the proportional relationship of gate dielectric capacitance and the current between source and drain , utilizing aluminum electrodes for an active matrix based array . Such metal inclusion restricts the tensile strains a device is capable of receiving without destroying the device. Other groups utilized metals in elastomers for capacitive sensing [16, 17, 23], limiting their elasticity. When considering the spatial resolution and ranges of these groups (Table 1.1), the density of sensors match the need density (>1 sensor / mm^2 [10]) for robotic fingertips where such values are desired.

3

Substrate	Range	Spatial Rez.	Conductive Matl.	Group
PDMS	0 - 131 kPa	1 mm^2	Copper	[23]
PDMS	0 - 160 kPa	3 cm^2	Gold	[16]
PU	1 kPa - 1 MPa	1 mm^2	Silver Wire	[17]
PDMS	50 kPa - 1 MPa	0.4-4mm^2	CNT	[18]

Table 1.1: Selected elastomer capacitive based tactile sensors

However, when scaling these sensors up to larger areas the conductive materials used can end up being quite costly and may not be as easy to manufacture for larger arrays. Multiple groups have investigated carbon black (CB) [20, 15] and carbon nanotube (CNT) doped PDMS [24, 20, 18, 25, 26] to create conductive PDMS (cPDMS) for tactile sensing. These materials are relatively inexpensive compared the noble metals utilized by [16, 17] and can provide adequate conductivity. Groups like Han et al. compared CB and CNT cPDMS to utilize in their tactile systems, and at equal weight percentage (14% wt.) CB cPDMS had a conductivity of 3.7 × 10^{-6} while CNT cPDMS had a conductivity of 4.3 × 10^{-2}S/cm). However, testing performed in the MicroRobotics lab has reported much higher conductivities of 4.6 × 10^{-2}S/cm for 15% wt. CB based cPDMS as seen in Figure1.2, which matches with similar results found by [27].

Additionally, the use of CNTs can still result in a somewhat high cost per sensor when comparing the conductive material gram for gram ($5.11/gm MWCNT Sigma Aldrich 724769 vs. $0.177/gm Carbon black Alfa Aesar 39724). While tactile sensing at a low cost is always a goal, at times pursuing a low cost solution without considering other criteria results in other limitations. Pugach et al. [28] utilized 3M Velosat conductive rubber, an inexpensive material utilized for over 20
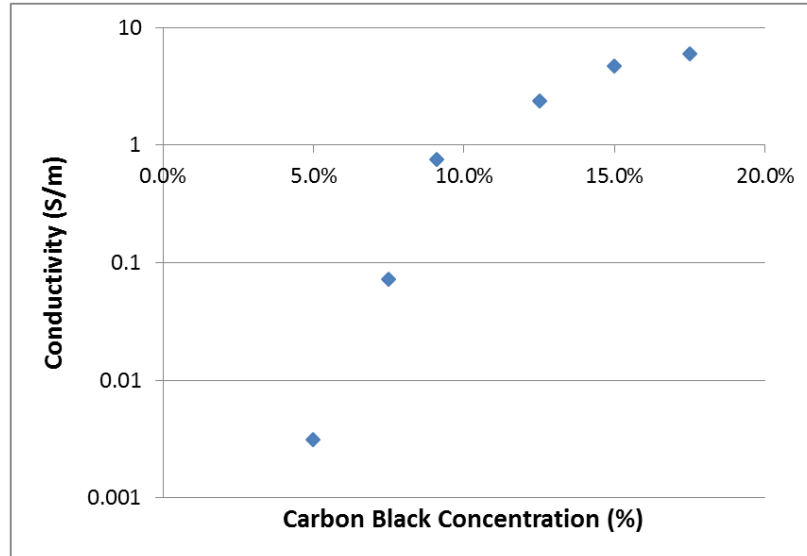
Figure 1.2: Conductivity of CB-PDMS versus carbon clack powder weight concentration

years in tactile sensing, but their tactile system was limited in only being capable of discriminating forces from conductive weights when compared to nonconductive weights [28]. Yet by utilizing existing commercial off-the-shelf (COTS) polymer sheets as a substrate and a conductive polymer mixture of CB and PDMS (henceforth referred only as cPDMS) to make a capacitive tactile array, a tactile sensor providing nominal force discrimination and spatial resolution can be realized while still keeping costs low.

While the threshold for touch force that can be perceived on the fingertip is 0.8 mN and under ideal conditions an indentation of 0.001 mm on human skin can be perceived (even more recently it was discovered humans are capable of perceiving nanoscale surface roughening in dynamic touch [29]) , a key concern is the location on the body where this distinction can occur [30]. For example, human perception

5

of point to point discrimination varies greatly when comparing a human hand to the lower calf , while such increased spatial resolution may not be required for larger areas on the human body [30, 31]. Concerns have also been raised regarding connecting tactile sensors to the neuromuscular system, questioning if the body is capable of receiving neural feedback from a prosthetic in greater quantities than a normal human body experiences [32]. An additional concern regards sensor "real estate", where sensors providing haptic feedback to another portion of the body to receive these responses has a limited surface area (e.g. prosthetic arm haptic feedback nodes connected to upper shoulder)[33]. While the system developed in this paper has not been used in prosthetics testing as of yet, large scale arrays can be highly useful for providing a spatial sensor density akin to human perception, preventing issues identified by [32]. Large scale arrays are available commercially from Tekscan and Takktile (Figure 1.3A & 1.3B) but such arrays typically cost $10s of dollars or more per sensor and additionally have their own calibration and flexibility issues [34, 35].
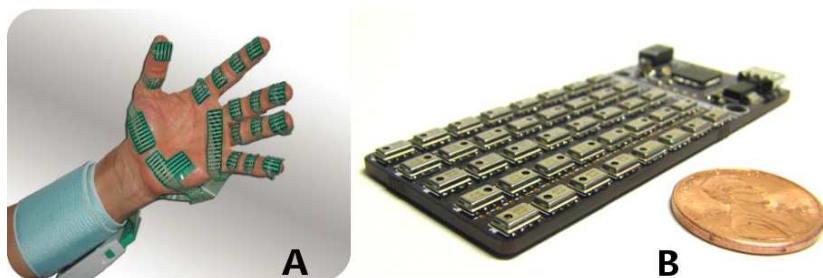
Figure 1.3: Commercially available tactile sensors by Tekscan (A) [3] and Takktile (B) [4]

The main goal of this research is to develop a manufacturing process that is compatible with elastomers for compliance and sensor flexibility while maintaining low cost for large area tactile arrays. Such sensors have been investigated for over thirty years, and through this timeframe researchers have refined the requirements needed to satisfy tactile sensing demands. The requirements outlined in this paper were aggregated from [36, 37, 10, 19] and are shown in Table 1.2 .

Requirement	Value
1.Detect a minimum force / pressure	1 mN / 10 Pa
2.Detect a range of forces /pressures	0 - 10 N / 0 - 100 kPa
3. Use little/no power	$\leq$100 mW per section
4. Durable	Capable of withstanding testing cycle $\geq$ 100x
5. Low in cost	$\leq$\$0.25
6. Spatial resolution similar to human skin	Approximately 1 sensor/mm^2 for fingertips and 1 sensor/5 mm^2 for palms and arms
7. Detect force direction	Force can be both normal and tangential
8. Low hysteresis	If sensor is saturated, must return quickly to its nominal shape ($\leq$30 s)
9. Short response time	Send information no later than 100 ms
10. Minimal wiring	
11. Minimal cross-talk	
12. Provide resilience against environment	Must not quickly fail if exposed to high humidity or water, capable of electronic shielding

Table 1.2: Requirements derived from research and use cases

The ranges desired for object manipulation (10- 100 kPa) and sensitive touch ($\leq$10 kPa) [19] were investigated in this project . By looking at inexpensive production methods such as roll to roll production or spray gun deposition often utilized in industry as well as investigating various inexpensive components such as COTS elastomer sheets and capacitive sensing chips the goals are to decrease the taxel (tactile pixel) cost to under \$0.25 each. This was in tandem with keeping the sys-

tem robust (e.g. strength of the whole apparatus, durability of the interconnects over testing cycles) and all while easily scalable to mass production. Conductive polymers were identified as a suitable route to accomplish this goal, and current sensors utilize cPDMS as a means to provide the conductive material.

A systematic overview of the tactile array and basic sensor design is discussed in Chapter 2 and multiple approaches to fabrication of these arrays are examined. The experimental setups and results are discussed in Chapter 3. Chapter 4 covers system concerns, future applications and provides final conclusions .

Chapter 2:   System Overview and Sensor Design

2.1   System Overview

When modeling the tactile system, it is important to highlight the system as if it were viewed from the user, in this case assumed to be a robot. In Figure 2.1 an interface connects to the sensing modules, with one layer of abstraction represented by the blue dotted boundary. These sensing modules themselves are further broken down into sensing chips, which take data from multiplexors, which receive data from sensor arrays comprised of taxels (tactile pixels) or capacitors. This also describes the method to which information is being passed, though worked backwards. This can be seen in Figure 2.2 , highlighting the activity of the sensing system when an object is placed on a set of taxels and can also be considered the ideal test case.

An object placed on an array depresses the elastomer taxels. This represents a change in capacitance, which is transmitted through the array and multiplexor to the sensing chip. This chip as a part of a sensing module then sends its converted information to an interface. Such an interface can help provide the user or tester a means to relate the once raw data back into 2-D or 3-D visualization, as seen in Figure 2.3. Here in Figure 2.3a and Figure 2.3d two items are placed across an array and via such an interface pressure profiles can be visualized in 2D (Figure 2.3b and
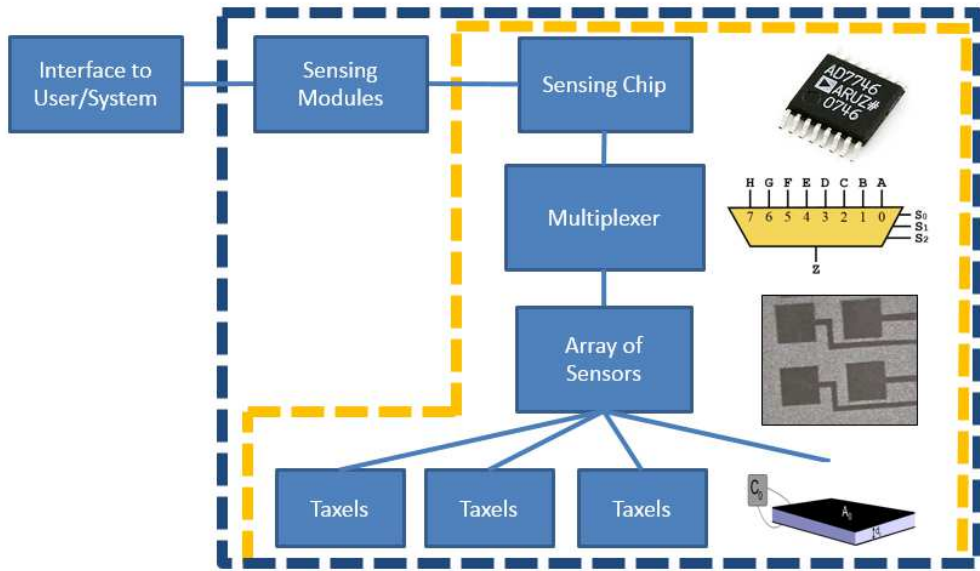
Figure 2.1: Tactile System Overview

A general system overview of a modular tactile system. Key subsystems include the capacitive sensing chip and its supporting electronics and the array of taxels comprised of dielectric and conductive elastomer materials.
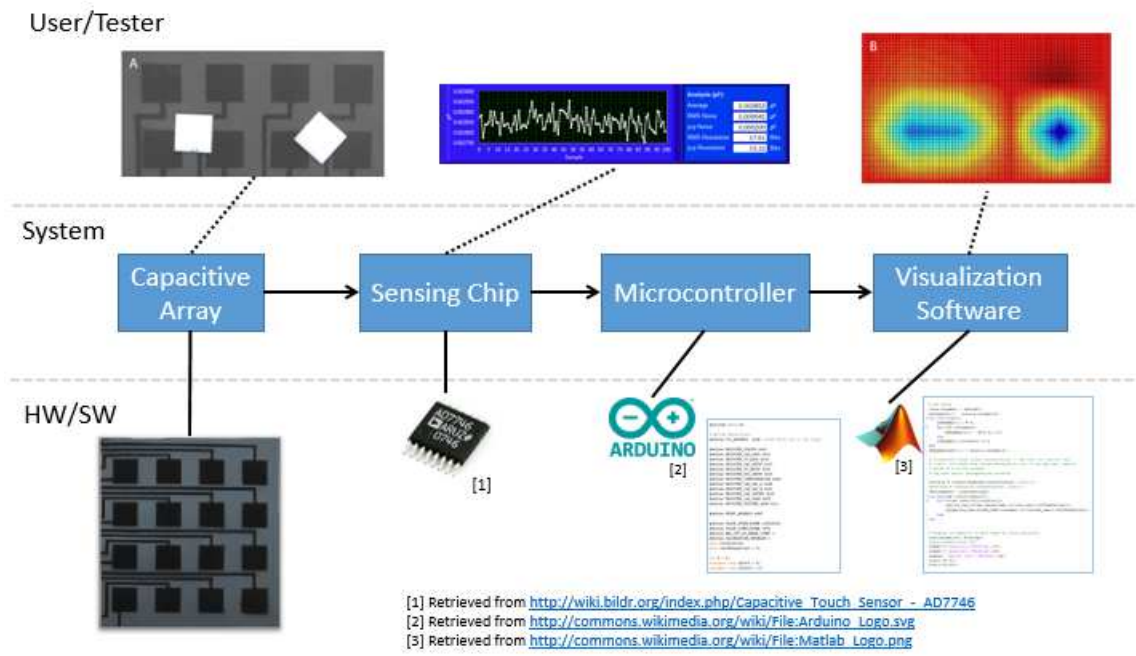
[1] Retrieved from http://wiki.bildr.org/index.php/Capacitive_Touch_Sensor_-_AD7746
[2] Retrieved from http://commons.wikimedia.org/wiki/File:Arduino_Logo.svg
[3] Retrieved from http://commons.wikimedia.org/wiki/File:Matlab_Logo.png

Figure 2.2: Information Flow

10
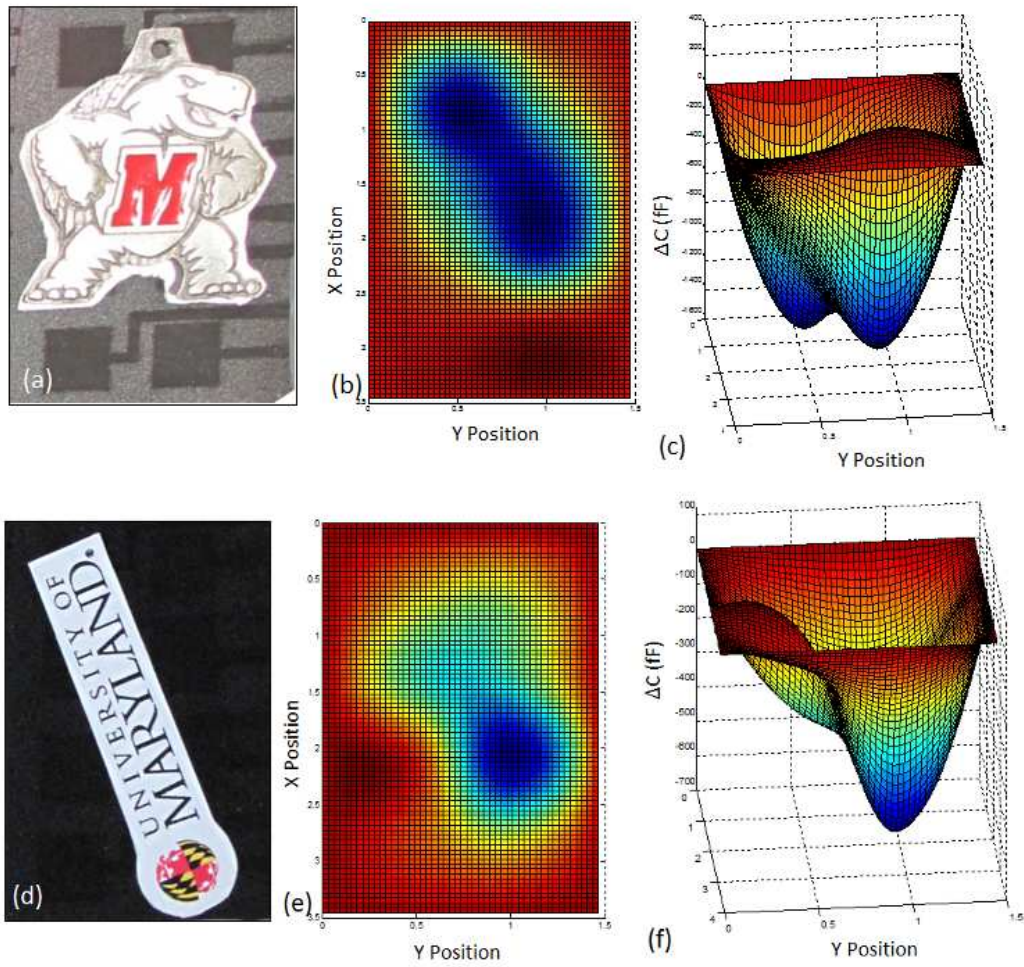
Figure 2.3: Object identification via visualization software
A cardboard-backed metal emblem (17.55 g) (a) and light decal (0.285 g) (d) are placed
across an array. Pressure profiles of the object are visualized via MATLAB code adapted
from [6] in 2-D (b & c) and 3-D (c & f) . Curvatures in the cardboard backing and decal
result in pressure profiles deviating from expected figure.

Figure 2.3e) or 3D (Figure 2.3c and Figure 2.3f).

Reviewing the requirements from Table 1.2 and literature [36, 18, 6], it can be seen that such systems would be best approached as modules capable of covering a large variety of surface areas and structures. Such modules must consist of components whose function and capabilities must trace back to the requirements of the system. This is immediately reflected in the fabrication process of such a system. Current efforts consider a spray deposition of cPDMS in a process outlined in Section 2.3, and with such a fabrication a variety of components can already be identified for simple scaling into mass production. For instance, the spraying mechanism/tool can be utilized repeatedly, as well as the stencil designs used to create a mask for conductive material deposition. Chips and multiplexors can be purchased en masse and can be part of a library of reusable components if desired, depending on the sensitivities of the chips, internal resistances of the multiplexors and the desired application or orientation. The elastomer material needed for the supporting structure and dielectric portion of the capacitive array as seen in Figure 2.4 can be created in the lab or easily purchased online, however these affect certain design factors and constraints in the system, and their relationships can be seen in Figure 2.5.
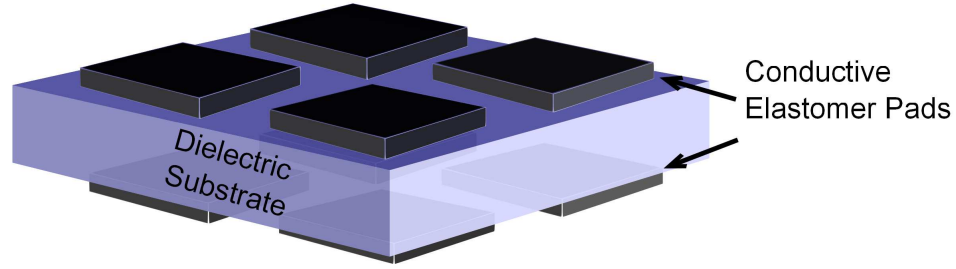
Figure 2.4: Simplified structure of tactile array
A visual diagram identifying patterned conductive elastomer pads on a dielectric substrate. Traces are removed and pad thickesses are exaggerated for visual clarity

The previous system overview from Figure 2.1 is broken down into two subsystems. The first is the array subsystem which includes the substrate and conductive material, and the second is the electronics subsystem, comprised of the capacitive sensing chip, multiplexer, microcontroller, and other components needed for electronic signal filtering. The main focus of the thesis work investigated the array subsystem, including constraints such as cost of array, the sensitivity of each taxel and the thickness of the dielectric, the last two being related as identified by a double sided arrow. Current work also is looking at increasing the range of sensor detection, which is related to chip sensitivity as well as to other constraints in the array subsystem. These inter-relationships continue to grow when looking at the whole system, and would be areas to investigate in future work. Within the array subsystem a tradoff example can be the comparison of the dielectric elastomer sheets either being created in the lab or purchased off the shelf. These sheets can be created in the lab by spinning uncured PDMS, resulting in uniform but very thin $\leq$ 200 μm sheets, but such thin materials are not as durable and can easily tear when

testing. Thicker sheets may be obtained in the lab via pouring into a mold and curing, this but may not be as consistent in thickness and thus reduce reliability of the sensor, and tactile array sizes are limited to the dimensions of the mold.
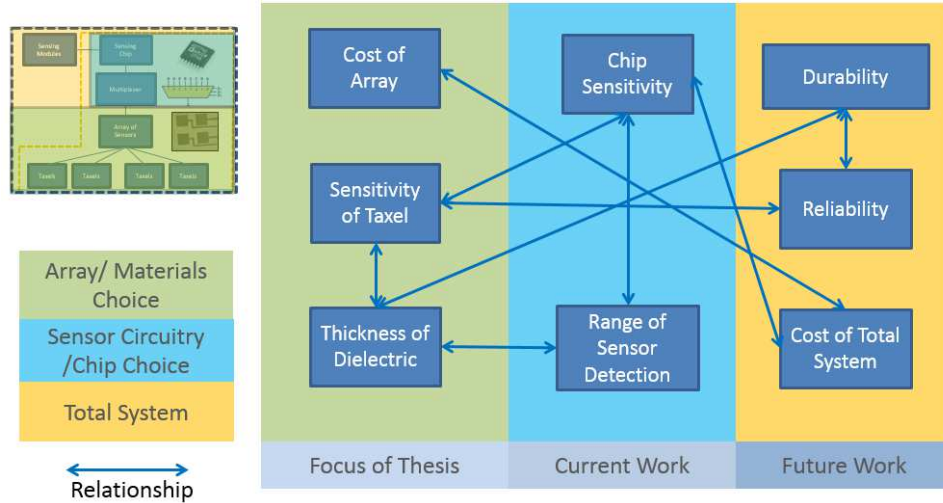
Figure 2.5: Trade-off issues of system and related research progress

Purchased sheets as the elastomer substrate can save time and increase reliability with guaranteed thickness tolerances of pm 10but come at a higher cost than those made in the lab. Thicknesses of such sheets can result in certain sensitivities as seen in Figure 2.5 that may affect chip choice. Such tradeoffs are important to outline, and by developing measures of effectiveness a proper design approach can be determined. It comes in to question how best to approach such inter-related constraints while keeping within the requirements. This was a challenging issue, and after several approaches were attempted, a simple weighted formula was created to determine the best outcomes. Tables 2.1, 2.2 and B.1 outline key areas of the design, and the resulting visual comparisons can be seen in Figure 2.6. It should be noted that the assessment of chip choice was made when the author was less experienced

14

with microcontrollers. Because the Silicon Labs (SL) C8051F996 is a microcontroller with added capacitive sensing function as opposed to the Analog Devices (AD) chip which requires a microcontroller to function it is recommended to re-evaluate the chip choice. The issues of programming difficulty in the SL chip resulted in the choice of the less complex AD chip, while very thin materials were determined to be limited in durability, identified in Figure 2.6, thus thicker materials were chosen. Finally, it was determined that due to the limitations of reliably creating elastomer sheets of a desired thickness in the lab, purchased elastomer sheets were the best option when designing a large area tactile array.

Sensing Chip	AD Chip	Value	SL Chip	Value
Power Reqs	Low	5	Low	5
Ω Limits	250 kΩ	2	Uncertain	2
Programmability	Normal	3	Difficult	1
Capacitive Limits	20 pF	2	Current-Limited	5
Cost	Low	4	Low	4

Table 2.1: Value comparison of capacitance chips

Thickness	$< 100~\mu$m	Value	100-500 μm	Value
Durability	Lower	1	Higher	4
Sensitivity	Higher	4	Lower	2
Range of Detection	0.1 Pa 10 Pa	3	50 Pa 800 Pa	3

Table 2.2: Value comparison of thickness ranges

Sheet Type	Lab Created	Value	Purchased	Value
Durability	High	5	High	5
Sensitivity	Dep. on Thickness	2	Dep. on Thickness	2
Reliability	Medium to Low	3	High	5
Range of Detection	Dep. on Thickness	2	Dep. on Thickness	2
Cost	Low	4	Medium to Low	3

Table 2.3: Value comparison of sheet type choice
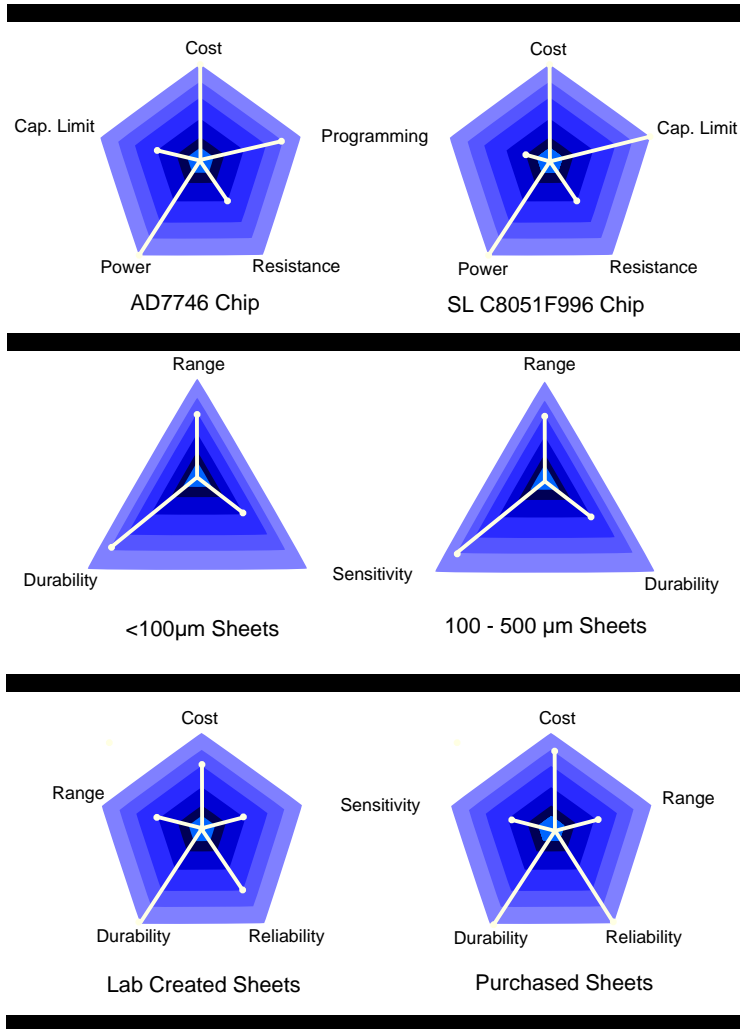
Figure 2.6: Tradeoffs across design choices

Values from Tables 2.1, 2.2, and B.1 are visualized in spider charts. The AD7746 chip, sheets 100-500 μm thick, and sheets purchased commercially were determined to be the best in value.

2.2 Sensor Design

To first order, we can assume than an elastomer-based capacitor can be modeled
as a simple parallel plate capacitor as seen in Figure 2.7. Thus when a force or
pressure is applied uniformly to the sensor, the sensor compresses vertically and
expands horizontally.
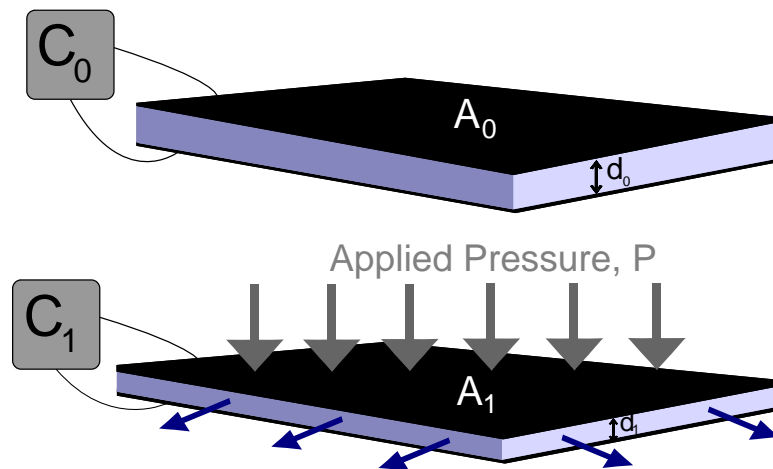
Figure 2.7: Flat plate theory

An elastomer-based capacitor is modeled as a flat plate. Pressure is applied
uniformly to the sensor, and due to the Poisson effect, the sensor compresses
vertically and expands horizontally. As the pressure increases the capacitance
increases proportionally.

Capacitance for a parallel plate is a relationship between the sensor area, the
dielectric thickness, and the relative permittivity of the material, while a change in
capacitance includes the Young's modulus of the material and the pressure applied,
as well as a capacitive gauge factor alpha. Assuming a constant pressure across the

area of the sensor, the change in capacitance can be calculated as

$$\Delta C = aC_0 \frac{P}{E} \tag{2.1}$$

with

$$C_0 = \frac{\epsilon_r A}{\epsilon_0 d} \tag{2.2}$$

where C_0 is the initial capacitance ϵ_r is the relative permittivity, ϵ_0 is the permittivity in vacuum, A is the sensor area, d is the thickness of the dielectric, P is the applied pressure, and E is the Young's modulus of the elastomer. While α should be 1 for isotropic materials with a Poisson's ratio of 0.5, previous research has shown that this factor is less than 1 in experimental measurements, and a value of 0.5 was used by Hu et al. in their experimentation [17]. For example, material values from a purchased 20A Durometer 10 mil thick sheet are $E = 843$ kPa and $d = 254$ μm. This in combination with the relative dielectric constant of PDMS estimated at $\epsilon_r = 2.65$, and the area of the sensor, $A = 1$ cm^2, should result in a theoretical sensitivity of 5.4 fF/kPa. This sensitivity along other calculated sensitivities will be compared later to experimental results in Chapter 4.

2.3 Fabrication

A variety of methods can be utilized to create all elastomer capacitive arrays. However, a main goal of this project was to prioritize the ease of fabrication as well as the overall cost of the design. This in turn brought other trade-offs that are

discussed later in the Characterization section. A pattern design was created in Solidworks and then cut into Delrin sheets via laser cutting (VersaLaser 3.60) . The sensor structure in Figure 2.7 requires both an elastomer dielectric and compliant electrodes. The elastomer dielectric used to generate the results in Chapter 3 are sheets of differing moduli, thicknesses, and textures purchased from McMaster Carr and Amazon Small Parts as outlined in Section 2.3.3. Part numbers for the materials are available in Appendix C. To create electrodes, a 17.5% wt. CB/PDMS mixture was used. Similar to Lipomi et al., the conductive electrodes are applied through spray coating [18]. The CB (Alfa Aesar 39724) is mixed in a 4:1 ratio of hexane solvent to total cPDMS mixture and stirred for 2 hours to reduce viscosity before spraying. Referring to Figure 2.8 a purchased elastomer sheet (step A) of chosen thickness and modulus is cut down to desired size. A stencil is affixed to the sheet and together are oriented vertically and affixed to pegboard to ensure an even spray deposition. A paint gun (Tool Force A-C2 HVLP) is used to spray the cPDMS and solvent solution onto the stencil-covered silicone sheet 3 times, with 3 second passes (step B).

The stencil is removed (step C) and the stenciled sheets are then placed in an oven at 125°C for 1 hour. Using a micrometer, the cPDMS layer was measured at approximately 50 μm thickness with a deviation of ±10 μm between batches. As seen in Figure 2.9, the sheets can easily conform to curved surfaces and are highly compliant. To create the full capacitor structure in Figure 2.8, a second electrode needs to be added. Following steps A-C, three separate designs were investigated, resulting in two design approaches of a double sided sheet, Design 1 (D1) and Design

3 (D3), and a design utilizing stacked single sided sheets, Design 2 (D2).
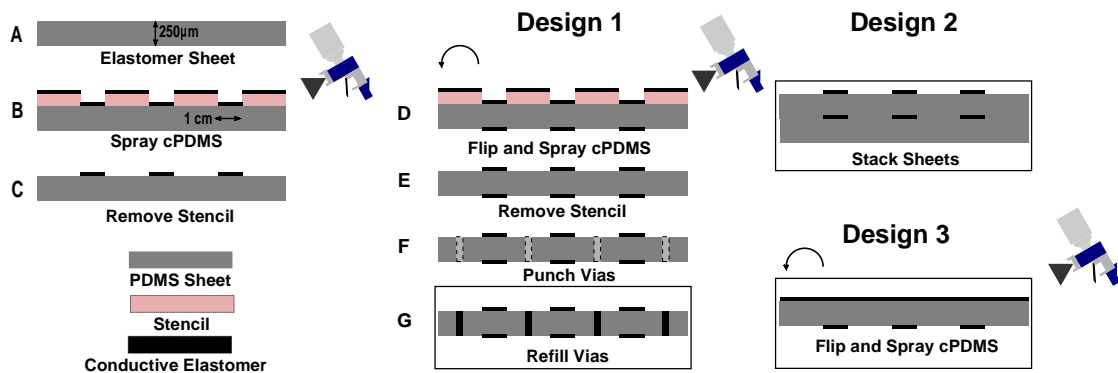
Figure 2.8: Fabrication processes for differing designs

Steps A-C are completed for each design, with the completed designs shown boxed.
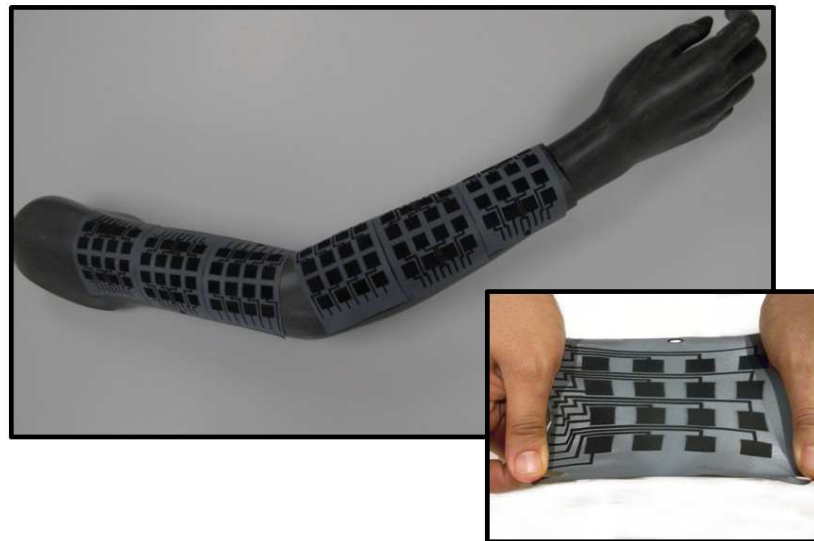
Figure 2.9: Conformable and flexible arrays

Sets of tactile arrays are placed along a mannequin arm, conforming to the curvature of the upper and lower portions of the arm. An inset shows an array being streched to approximatley 175% of its original length.

2.3.1   Double Sided Sheets

In the first approach, the patterned silicone sheet was flipped over and the same process was repeated to deposit cPDMS on the opposite side of the sheet as shown in step D of Figure 2.8. At the time of this design production, stencil patterns differed from later designs, as seen in Figure 2.10. Figure 2.10 A was composed of two 4x2 arrays with traces leading out to opposing sides of a sheet, and whose stencil did not include alignment holes. Instead, the two sides were aligned visually. Spacing between the pads was 5 mm and traces 1.5 mm in width were spaced 5.08 mm apart for convenient header connection.
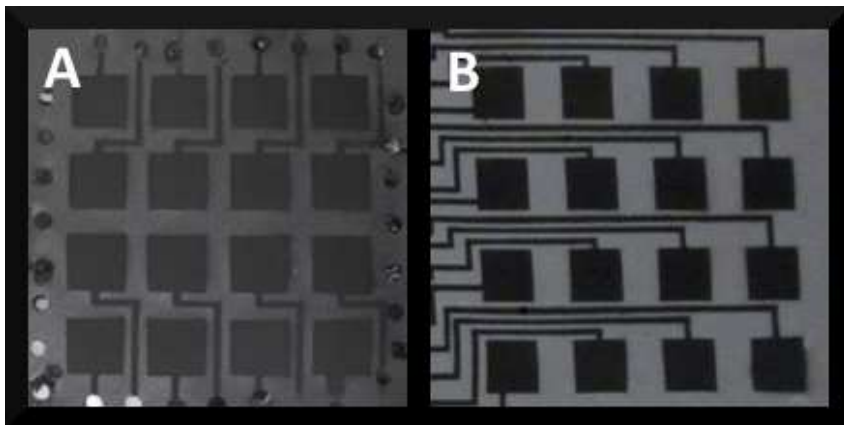
Figure 2.10: Differing patterns utilized in stenciling
Tactile arrays with a double sided pattern were initially developed with multiple vias bordering the array seen in (A). Arrangement of traces to taxel pads along one side of an array reduced via connection requirements (B).

Figure 2.10 B is a 4 x 4 array with all traces leading to one side of the sheet whose stencil had alignment holes. This was created to reduce pin connections and to connect to a custom board developed for module testing, discussed later in Section 3.6. Traces were reduced to 1 mm in widthand spacing between pads

21

were increased to 7.5 mm to allow all traces to fit between rows of taxels. Further decreases in trace width resulted in resistances greater than 100 kΩ and would not function with the capacitive sensing chip. Due to these distinguishing differences further design clarification will identify the pattern used in Figure 2.10A as Design 1A (D1A) and the pattern used in Figure 2.10B as Design 1B (D1B).

In the D1A design, vias were punched to connect the two layers and refilled. The 17.5sensors to pads on the edge of the sheet were measured between 1.5 and 35 kΩ.The advantage of this process was that a single dielectric sheet is used to create the sensors. However, the additional steps required to punch the vias and align the front and back layers added complexity, and the vias themselves often separated from the dielectric elastomer sheet after multiple tests, also seen in Figure 2.10A . The D1B design improved upon this by utilizing alignment holes designed and lasercut in the stencil pattern. The patterned stencils were aligned on on both sides of sheet during the spray application and pad alignment was confirmed by light transmittance through the thin and transparent sheets. Thicker and opaque sheets were placed between matching stencil patterns to confirm exact sensor pad overlap. Traces were also connected along the backside, as highlighted in Figure 2.11. With finer traces, series resistances connecting the array sensors to pads on the edge of the sheet were measured between 37 and 76 kΩ.

The advantage of these processes are that a single dielectric sheet is used to create the sensors. However, in both D1A and D1B designs, each resulting sensor has a slight curvature so that it bows up from the plane of the silicone sheet. The effect is enhanced if additional layers of PDMS mixed with solvent (but without car-
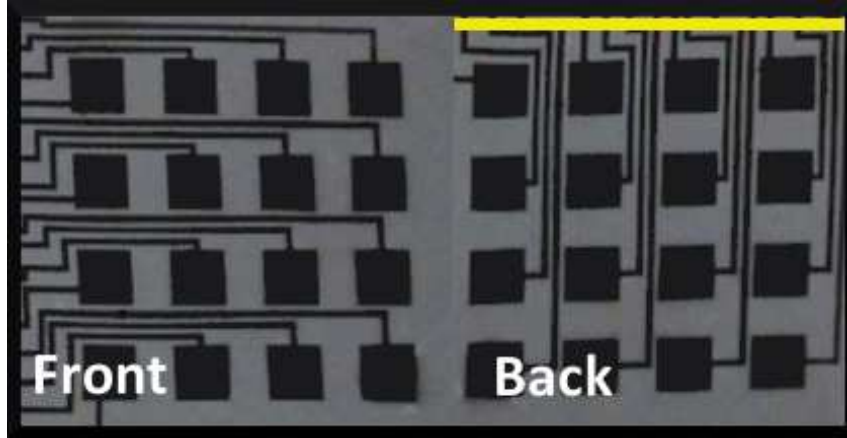
Figure 2.11: Front and back sides for D1B pattern stencil. Sensor pads on the back are connected via a highlighted single trace.

bon) are sprayed on the sensor array as seen in Figure 2.12a. These bumps clearly deviate from the simple flat capacitor model when pressed as shown in Figure 2.12b. While the cause for this bowing is still unknown, it is likely the result of the solvent in the cPDMS mixture causing swelling when sprayed on the silicone, which is discussed later in Section 3.7. Another design approach, D3, reduced the fabrication complication of vias by fully spraying the underside of the patterned sheet with cPDMS. While this reduced fabrication complexity and circuitry connection, it brought on other issues which will be discussed further in section 3.7.

2.3.2 Single-sided sheets

A second approach is to simply stack two sheets with electrodes patterned on one side as shown under Design 2 of Figure 2.8. Curved bumps are still seen in this single side process, but they are less noticeable. Series resistances connecting the array sensors to pads on the edge of the sheet were measured between 7 and 70 kΩ.

Sensor Side Profile

(a) Bump formed after PDMS spray coating

(b) Exaggerated total sensor side profile and deformation with mass load
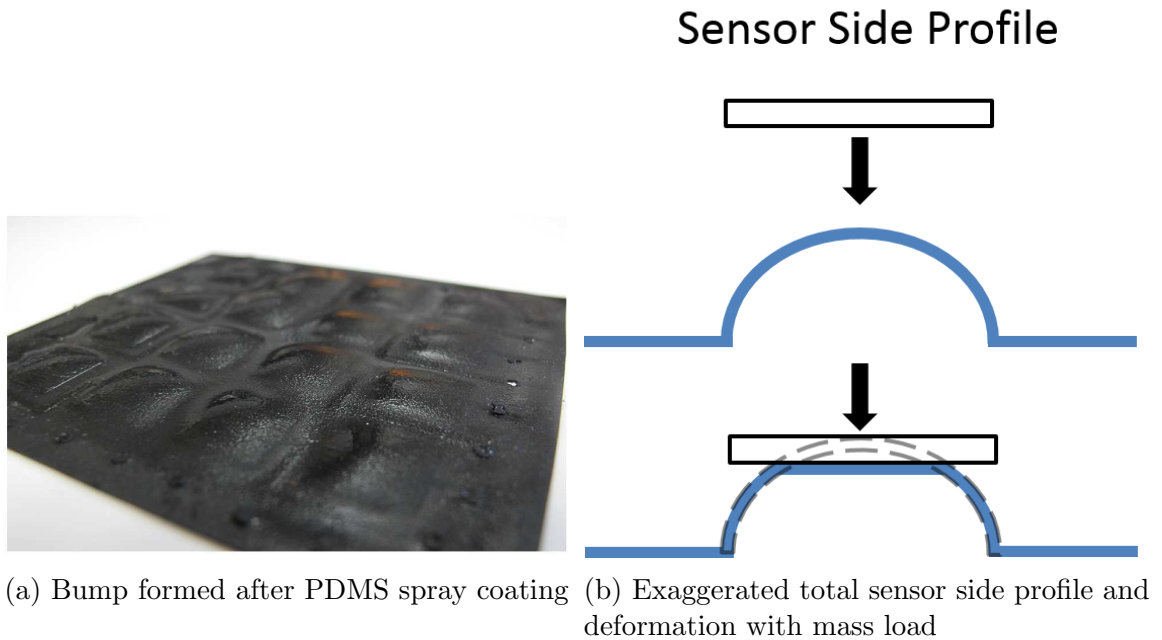
Figure 2.12: Textured features on capacitive arrays

While simple to assemble, there is no adhesive used to connect the two layers at present.

2.3.3 Materials

Testing was done for an assortment of different requirements. This included force and capacitive relationship modeling, bandwidth testing, spatial resolution testing, and environmental/durability testing which will be covered in Chapter 3. One of the most important tests was determining the force to capacitance model for various off the shelf materials. Table C.2 outlines the materials comparing normal force to capacitance. Both Amazon Small Parts (ASP) and McMaster Carr (MMC) identify their materials by Shore A Hardness and mil thickness. For convenience these have been converted to their their thicknesses in μm and their Young's Modulus in MPa

via the equation

$$E = e^{0.0235S - 0.6403} \tag{2.3}$$

where E is the Young's Modulus of the material in MPa and S is the Shore A hardness. Literature is limited in suitable conversion models for Shore A hardness values under 40 [38, 39, 40],however this equation has been identified to be suitable for conversions of Shore A hardness values from 20-80 [41] and was utilized in this research. Henceforth all future graphs and discussions will reference the material by its modulus and thickness in these units.

2.4   Converting Capacitance to Digital

Kovacs identifies that capacitance can be measured in a variety of ways, be it with charge-sensitive amplifiers, charge-redistribution techniques, impedance measurements, RC oscillators, or direct charge coupling [42]. The AD7746 is a 24 bit 2 channel $\Sigma - \Delta$ capacitance to digital converter identified in its technical specification sheets as a "high precision converter consisting of a second order ($\Sigma - \Delta$ or charge balancing) modulator and a third order digital filter", which utilizes charge amplification as discussed below [43] . It has a maximum sampling rate of 90.9 Hz (11 ms), and a minimum of 9 Hz (109.6 ms). However actual performance based on measurements has shown limits of 15 bit resolution at 90 Hz. With a range of ± 4.096 pf this results in a resolution of 0.25 fF. It also is capable of a capacitive offset of up to 16.87 pF, allowing the chip to measure up to 20.966 pF. Its limita-

Material	Backing	Texture	Thickness μm (mil)	Hardness Shore A	Young's Modulus (MPa)	Supplier	cPDMS Adherent
Silicone (grey)	none	slightly mottled	254 (10)	10A	0.667	ASP	Yes
Silicone (black)	none	slightly mottled	254 (10)	20A	0.843	ASP	Yes
Silicone (black)	none	slightly mottled	381 (15)	20A	0.843	ASP	Yes
Silicone (orange)	adhesive backing	smooth	794 (31.25)	10A	0.667	MMC	Yes
Silicone (orange)	adhesive backing	smooth	794 (31.25)	20A	0.843	MMC	Yes
Silicone (orange)	adhesive backing	smooth	794 (31.25)	30A	1.07	MMC	Yes
Silicone (white)	none	smooth	1588 (62.5)	50A	1.71	ASP	Yes
Silicone (orange)	none	smooth	794 (62.5)	60A	2.16	MMC	Yes
Silicone (orange)	none	smooth	794 (31.25)	70A	2.73	ASP	Yes
Foam Rubber (orange)	none	dense diamond pattern	1575 (62)	N/A	(0.621-0.896)*	ASP	No
Latex	none	smooth	381 (15)	30A	1.07	ASP	No
Neoprene Rubber	none	smooth	1588 (62.5)	60A	2.16	ASP	No
Styrene-Butadiene Rubber	none	smooth	1588 (62.5)	75A	3.07	ASP	No

Table 2.4: Materials varied in properties of modulus, thickness, and surface roughness.

* Material listed as medium-firm, both medium and firm having differing moduli

tions in conversion rates due to oversampling may result in further investigation of a custom made low-cost capacitance-to-digital converter as seen in the work of Cheng et al. [44], though possibly at the cost of lower signal to noise ratio. A review of how Sigma Delta conversion provides accurate measurement is provided in Appendix D.

The AD7746 is identified in its technical specifications that the chip has resistance limits of 10 kΩ before significant error in readout occurs for capacitive measurement [43]. However, testing was done to verify this limitation, and it was found that resistances up to 250 kΩ resulted in 0-5% variation in capacitive measurement (1-5 fF up to 100 kΩ, up to 84 fF at 250 kΩ, >500 fF at higher resistances). This aids in the flexibility of the sensor system, allowing for less conductive (and less expensive) materials to be used.

Chapter 3:   Testing Results

3.1   Experimental Setup

An assortment of materials were compared for testing and can be referenced in Table C.2. These ranged in moduli, thicknesses, and material composition. Each testing area utilized a custom-made testing apparatus tailored for the desired information. In order to profile the capacitive response of these arrays a simple cantilever beam was used to place various forces on a given sensor. A small 1cm^2 Delrin square was used to distribute the force over the whole sensor. For lower pressures small 1 x 1 cm Delrin squares were stacked on top of the sensor. These changes in capacitance were measured via probes that were secured into place via Styrofoam puncture as seen in Figure 3.1a. The probes were connected to an AD7746 Evaluation Board, and this sensing information was then collected and visualized in MATLAB as overviewed in section 3.3. In order to measure the bandwidth response of the tactile sensors, a custom-built stand with a motorized arm powered by an Ardunio microcontroller with a motor shield was utilized as seen in Figure 3.1b. The motor shield provided an integrated L293D motor driver allowing for programming of the stepper motor at various speeds. The probes were again connected to an AD7746 Evaluation Board, while the Styrofoam board platform holding the

28

array and probes was placed on a load cell (Transducer Techniques GS0-1k) calibrated for weight loads of 0-1 kg. The load cell was connected to an Arduino Mega microcontroller for voltage readout and force comparison. Lastly a system comprised of a custom circuit board seen in Figure 3.1c & 3.1d (EAGLECAD design discussed in Appendix B) and Arduino microprocessor (Sparkfun Arduino Pro Mini 328 - 5V/16MHz with FTDI Basic Breakout - 5V board) with a bag clip was utilized to measure spatial resolution from varied modules. The custom circuit board was manufactured by OSHPark. The coding utilized to communicate with the AD7746 chip was adapted from the Interactive Matters code that can be found at (https://github.com/interactive-matter/Arduino—AD7746) and a link to the updated code is attached in Appendix A.

3.2 Characterization

An example of an array is seen in Figure 3.2. This array was created via the D1A design as identified in Section 2.3.1. One sensor in this array is capable of detecting 0.5 mN up to 2.5 N (0.5 Pa - 25 kPa), this being akin to feeling the resting weight of a housefly all the way up to a large grapefruit on just one sensor. This large area design has a spatial resolution of 1 sensor/cm^2 which at the moment does not fulfill the requirements from Table 1.2 but utilizing interpolation through a program such as Matlab ,approximations of object locations can be determined without objects directly being on top of a sensor. Fabrication with these materials purchased in relatively small quantities results) in a cost of less than $0.12 per
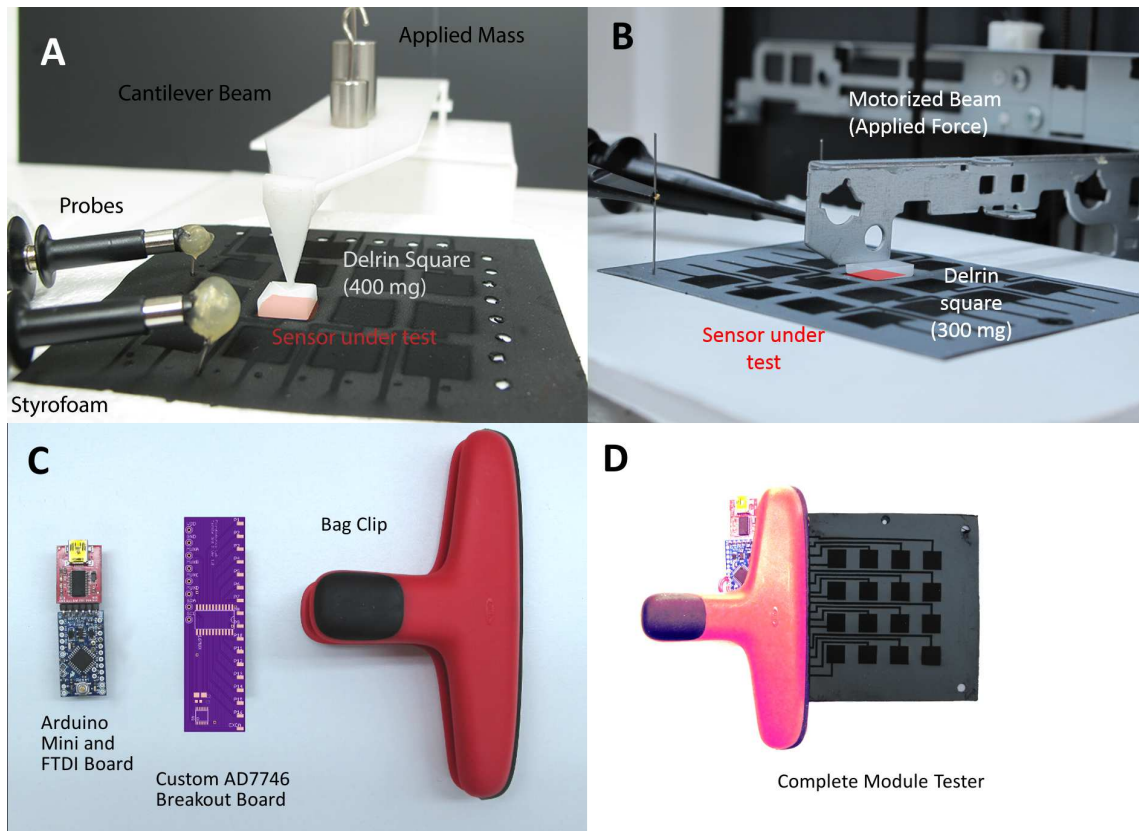
Figure 3.1: Static force testing apparatus (A), bandwidth testing apparatus (B), and current ZIF-like connector (before assembly in (C)) for spatial resolution testing (D)

sensor.(A calculation is provided in Appendix D).

3.3 Static Force Testing

The response of the capacitive sensors to static loads was tested using the apparatus shown in Figure 3.1A. Static force testing was done on the D2 (single sheet) , and double sided designs, D1A, D1B & D3, with previous work incorporated from [5] utilizing 0.843 MPa 255 μm thick sheets in both D1A & D2 designs.Three separate taxels were tested on each array three times at varying pressures, and the data for

Specification	Value
Substrate	0.84 MPa 250 µm Silicone
Conductive Material	Carbon Black / PDMS
Array Size	(4 x 4) 5.5 cm x 5.5 cm
Range	0.5 mN - 2.5 N (5mg – 250g)
Spatial Resolution	1 Sensor/cm^2

| 5 – 10 mg | 100 – 400 mg | 2 - 5 g | 30 - 50 g | 100 - 150 g | 250+ g |

Mass ➡
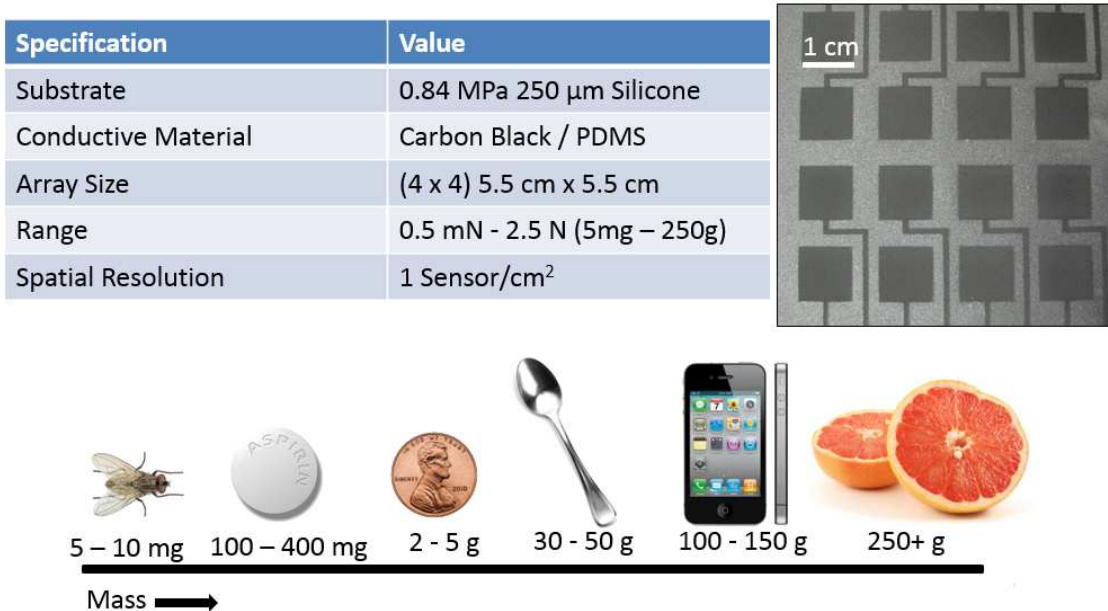
Figure 3.2: Prototype profile

each pressure from each taxel was averaged. The experimental data is compared against the theoretical capacitance based off of equation 2.1 and is approximated via the Taylor series simplification, assuming a linear relationship and considering the secondary derivative negligible to obtain

$$\Delta C = C_0 \frac{FA}{E} \tag{3.1}$$

$$\Delta C = \epsilon_r \frac{FE}{d} \tag{3.2}$$

Where F represents the force in Newtons, E is the modulus in Pa, ϵ_r the dielectric constant in $\frac{Farad}{m}$, and d the thickness of the sheet in meters.

A characteristic found with the bump formation on the arrays was an increased change in capacitance. To better visualize the comparison of experminal data to

31

theory, a capacitance offset was utilized when measuring these sensor arrays. As seen in Figure 3.3 , capacitance changes at low pressures do not match the theoretically expected slope, represented by a dashed line, for a sensor on a 0.843 MPa 255 μm D1A patterned array, and this is likely due to the bump feature as described earlier.

Materials stacked onto the bump begin to compress it back to a flat form, and a linear slope can be seen by the dotted line, representing the best linear fit to data. Intial experimentation to determine the pressure required to flatten the bump feature resulted in taring out a capacitive offset value equal to the force of approximately1 kPa as reflected in Figure 3.5, however recent testing has found that
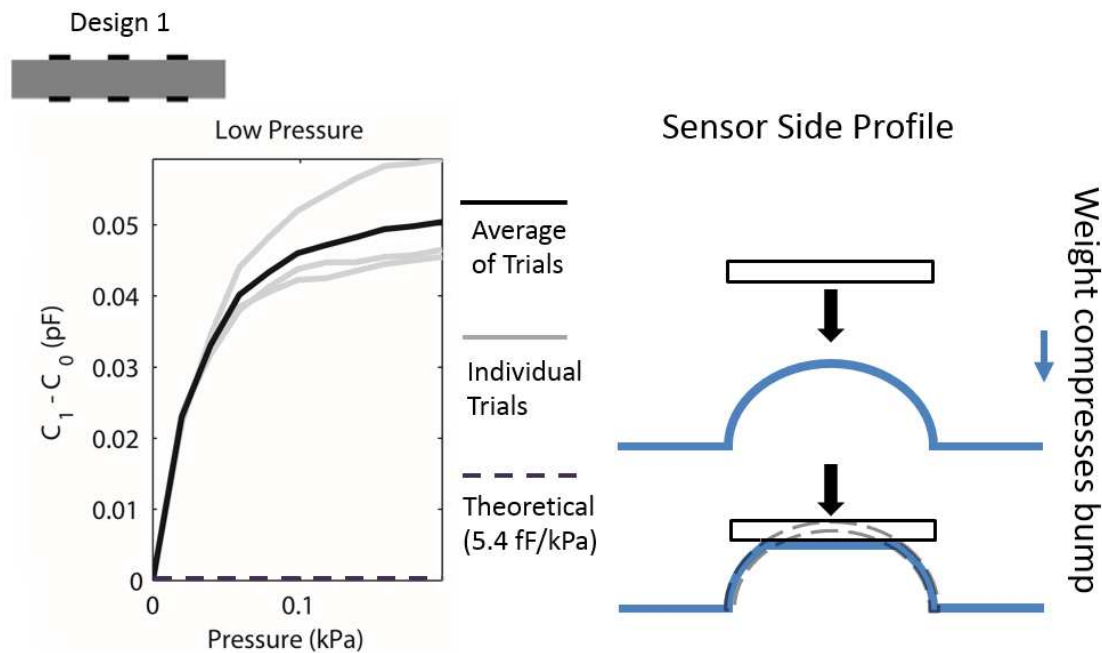
Figure 3.3: Low pressure data from a 0.843 MPa 255 μm D1A patterned array [5]

300 mg Delrin squares are stacked onto a sensor and begin compressing the bump feature, resulting in a change in capacitance that deviates from theory.

if a capacitive offset value equal to the force of 40 Pa, i.e. a mass of 400mg to flatten

the bump, is removed from the baseline, the resulting experimental data matches in

slope with the expected theory at the pressure range of 0 - 25 kPa. This capacitance

offset approach will be utilized later in other data comparisons.
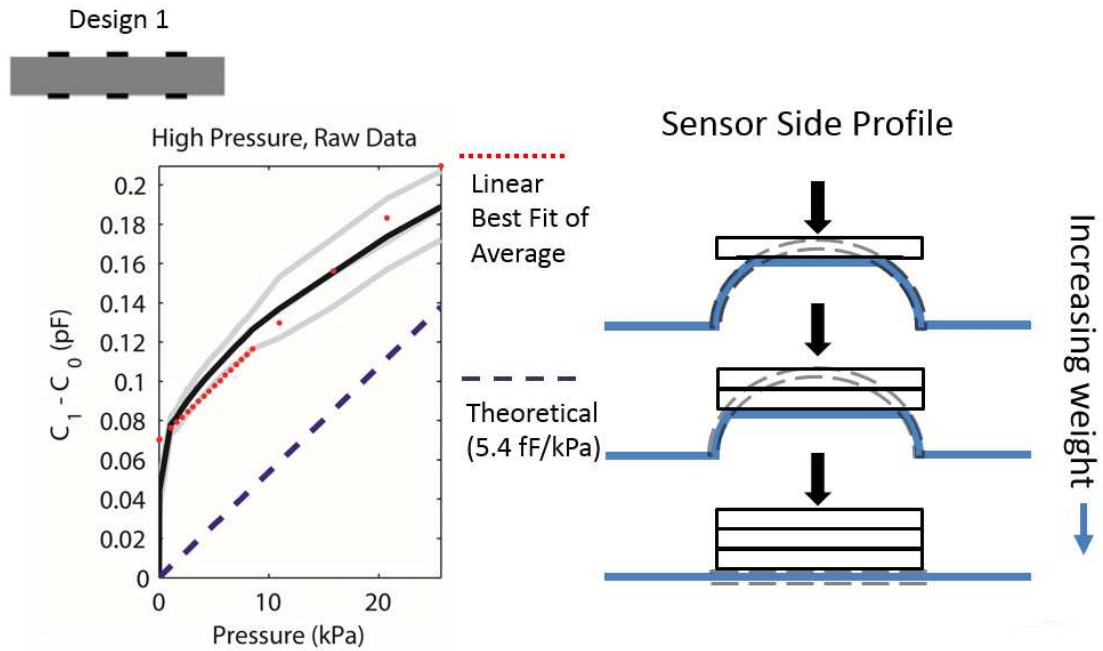
Figure 3.4: High pressure data from 0.843 MPa D1A patterned arrays
[5]

As the pressure increases the increased pressure flattens the bump feature, and the
change in capacitance begins to approach a linear slope.
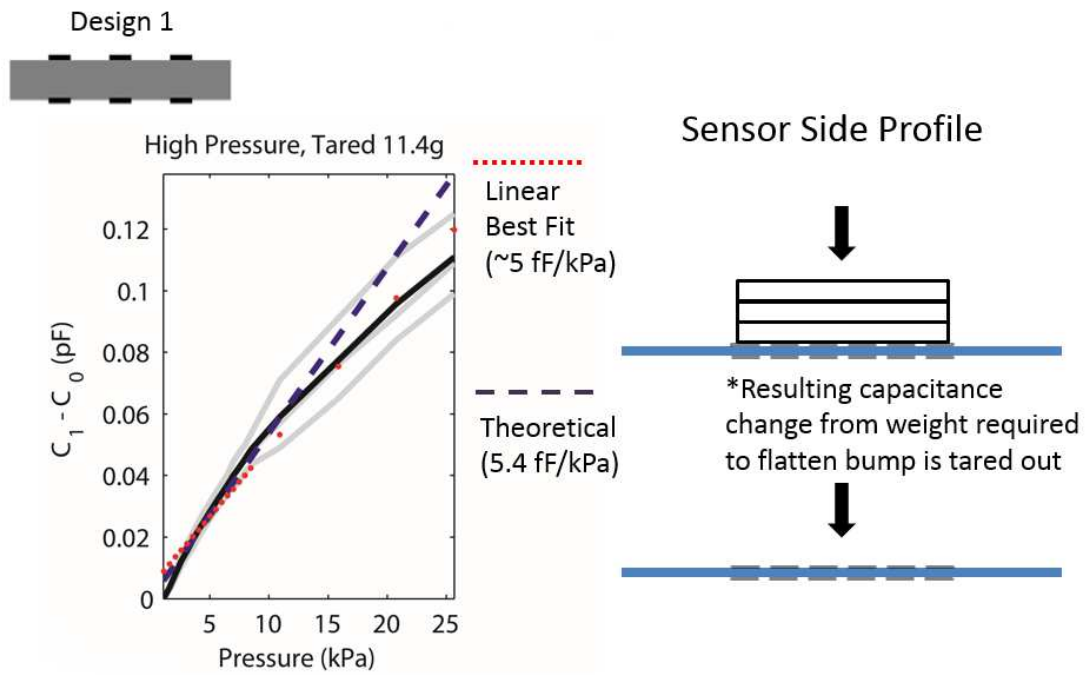
Figure 3.5: High pressure data adjusted with capacitance offset from 0.843 MPa D1A patterned arrays [5]

A capacitive offset value equal to the pressure expected to flatten the bump feature is removed from the baseline. The resulting experiments slope matches the theoretical change in capacitance.
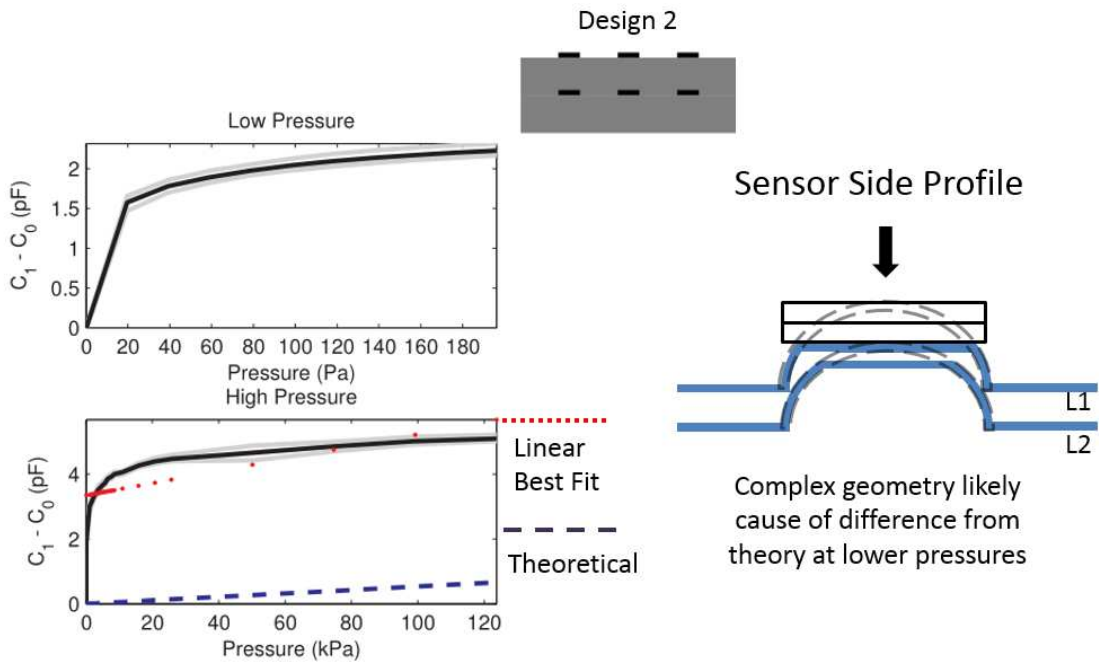
Figure 3.6: Low and high pressure data from 0.843 MPa single sided stacked sheets [5]

The stacked array design, D2, was also compared against the theoretical slope in an array comprised of 0.843 MPa 250 μm sheets. The design deviated from theory, though as seen in the high pressure figure the linear best fit seems to match well in slope with the theory as seen in Figure 3.6. This extensive increase in capacitance is suspected to be due to the complex geometries that may be occurring with two bumps stacked on top of each other as seen in the sensor side profile. This arrangement is likely also the reason for a high sensitvity as seen in Figure 3.7, where 5 mg uniform fragments obtained from the lasercut Delrin stencils were placed onto an array. A total of thirteen fragments were placed on a sensor, resulting in a pressure of approximately 6.5 Pa. The standard deviation across eight separate

sensors demonstrates the sensitivty to be consistent amongst the sensors. While this design was simple to assemble, delamination was a consistent issue, and this design was not investigated beyond static testing.
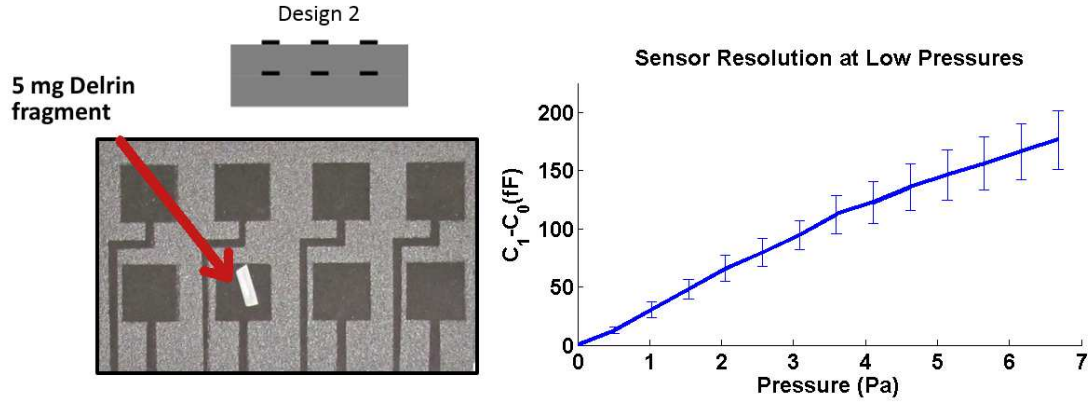
Figure 3.7: Sensor resolution at 0.5 Pa is witnessed on a D2 array comprised of 0.843 MPa 255 μm sheets [5]

As all testing of D1A has been reviewed, the remainder of the work will refer the D1B pattern as the D1 array for simplicity. All arrays in the remaing comparisons had deviations of approximately $\pm$ 7 fF up until 100 kPa, upon which deviation expanded to approximately $\pm$ 40 fF . When comparing materials with adhesive backing, which all had the same thickness of 1587.5 μm, both 0.667 and 0.843 MPa sheets had nearly the exact same profile, possibly being the same modulus sheets simply mislabeled by the manufacturer . All arrays had deviations of approximately $\pm$ 7 fF up until approximately 100 kPa, upon which deviation expanded to $\pm$ 40 fF. As with all arrays tested at low pressures, the adhesive backed sheets deviated from theory as seen in Figure 3.8. Additionally, as seen in the lower portion of Figure 3.9, the 1.07 MPa sheet is nearly parallel with the theoretical model, highlighting the

36

possibility that with higher moduli and thicknesses, the experimental may match

well with the theory.
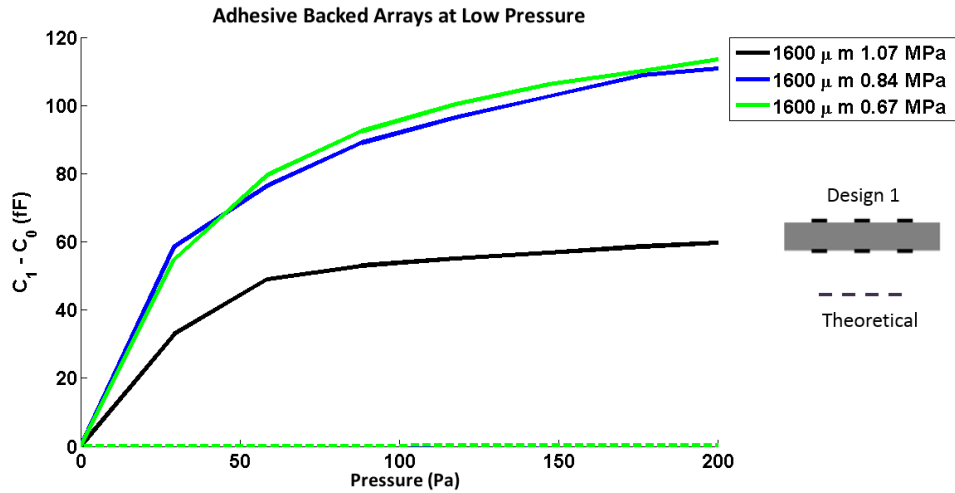
Figure 3.8: Arrays with adhesive backing and differing moduli are tested at low pressures
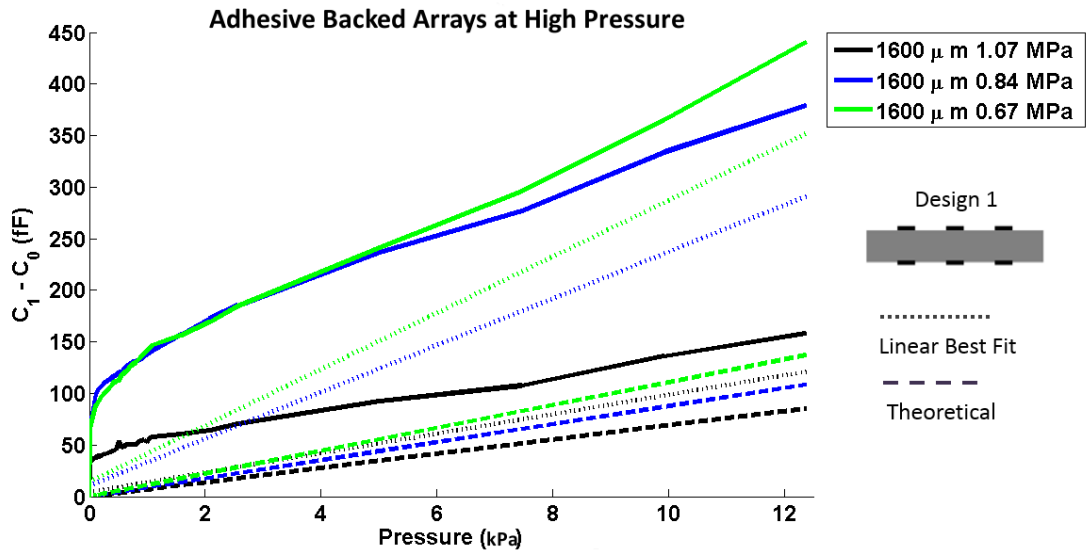
Figure 3.9: Arrays with equal modulus and differing thickness are compared at high pressures

This indication is further reinforced in Figure 3.10 where design patterns D1 and D3 were compared with the same thicknesses and modulus, as it can be seen that all experimental and theoretical data are parallel. A noted deviation is the increased capacitance readouts of arrays patterned with one side fully coated with cPDMS compared to the double patterned arrays. It is highly likely that the fringe capacitance that was negligible in the equally dimensioned parallel plate, but with a solid backing below, the plates extend along the traces. This highlights an issue with this design, which may lead to ruling it out in future design iterations.

Lastly, a notion to compare materials of thicknesses below 1 cm resulted in Figure 3.12 which identified a relationship between material modulus and adherence to the theoretical model. While materials of low modulus and small thicknesses ($\leq$ 500 μm) revealed experimental data with slopes divergent from theory, the 2.73 MPa 793 μm thick array had a slope that was in parallel with the theory. An added interesting revelation was that at the low pressures (seen in Figure 3.13 the 2.73 MPa material was the only data which had a linear slope as opposed to a logarithmic slope seen from the other materials. This leads to the hypothesis that such a stiff material was not subjected to a drastic bump formation found in lower modulus materials, yet it still has high sensitivity that deviates from the theoretical.

Reviewing the materials in Table B.1, there is no clear pattern in what materials and patterns are best suited for matching theory, with an assortment of materials deviating approximately 30

Another area of interest was improving the capability of the sensor array to accurately measure pressure profiles of conductive materials. Testing was performed
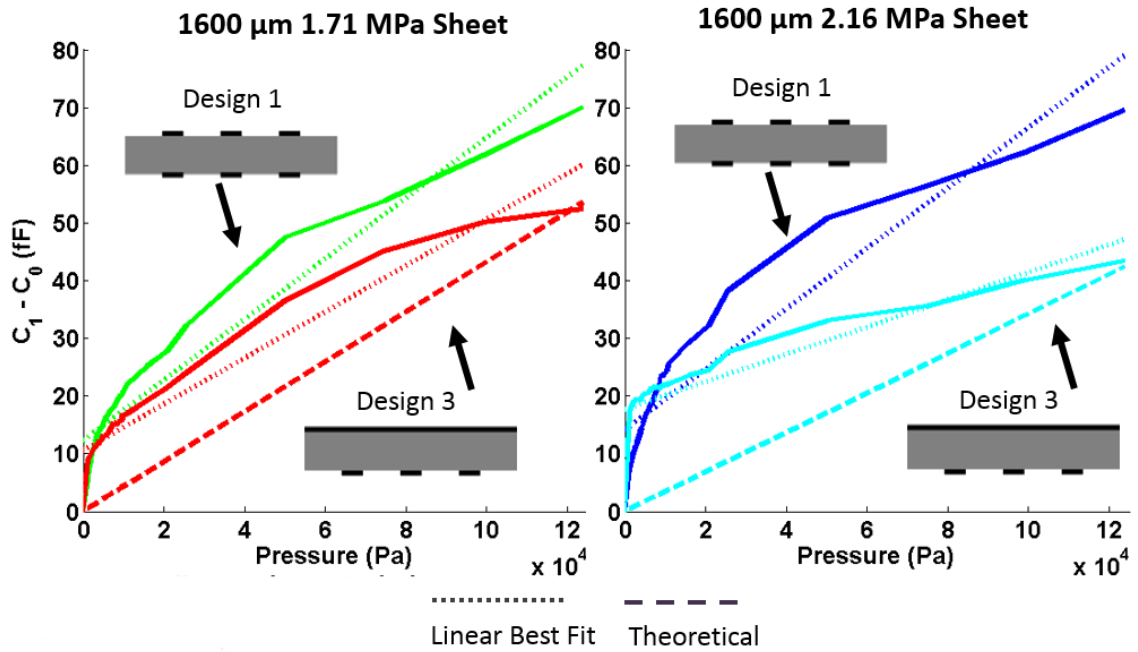
Figure 3.10: Arrays with differing patterns and equal modulus are tested at high pressures

Note: All data shown includes 400 mg offset

	Materials		% divergent from theory	
Pattern	Modulus	Thickness	No Cap.	400mg Cap.
	(MPa)	(μm)	offset	offset
D1	2.73	800	205	225
D1	2.16	1600	50	53
D1	1.71	1600	20	21
D1	1.07	1600	36	37
D1	0.84	1600	159	164
D1	0.84	400	36	35
D1	0.84	250	43	42
D1	0.67	1600	146	149
D3	2.16	1600	38	31
D3	1.71	1600	11	8
D3	0.67	250	44	43

Table 3.1: Experimental deviation from theory among tested arrays
Arrays composed of varying thickness, modulus and design pattern are compared against theoretical capacitance.
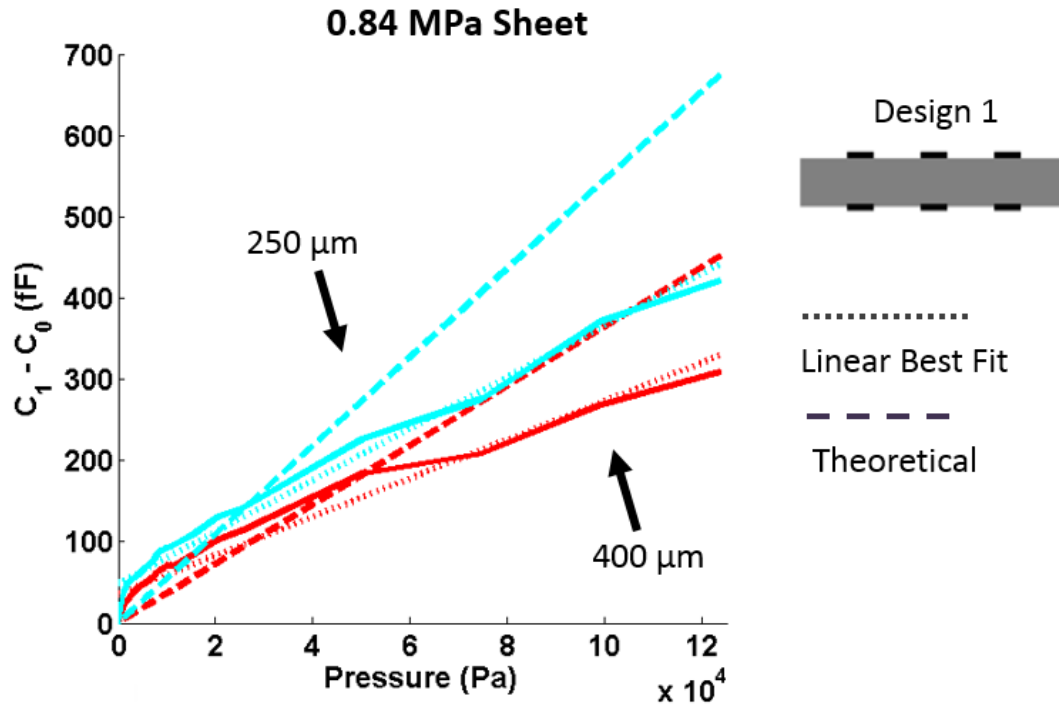
Figure 3.11: Arrays with differing thicknesses and equal modulus are compared at high pressures

Note: All data shown includes 400 mg offset

on a set of sensor arrays to determine if PDMS coating would prevent conductive materials from shorting the cPDMS sprayed sensor when in contact. The set of arrays were all based on 0.843 MPa 255 μml sensor sheets with a D1A design. Three separate taxels were tested on each array three times at varying pressures, and the data for each pressure from each taxel was averaged. One array was not coated with PDMS, and was considered the control. A second array was sprayed in the same fashion as the fabrication method outlined in Section 2.3 with 4:1 hexane to PDMS and seen in Figure 2.12, and had a deposited layer of PDMS approximately 45 μm thick with a deviation of $\pm$15 μm. The third array was embedded between
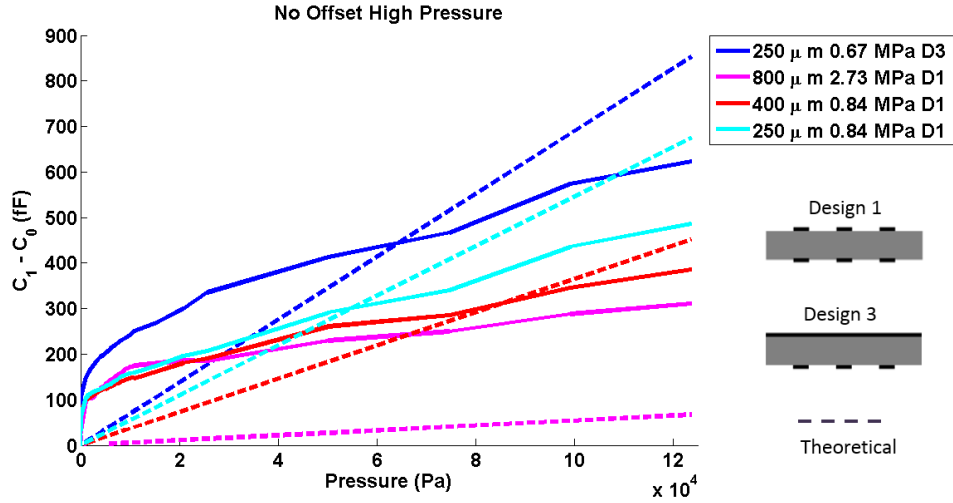
Figure 3.12: Sheets with thicknesses below 1 cm and differing moduli are tested at high pressures
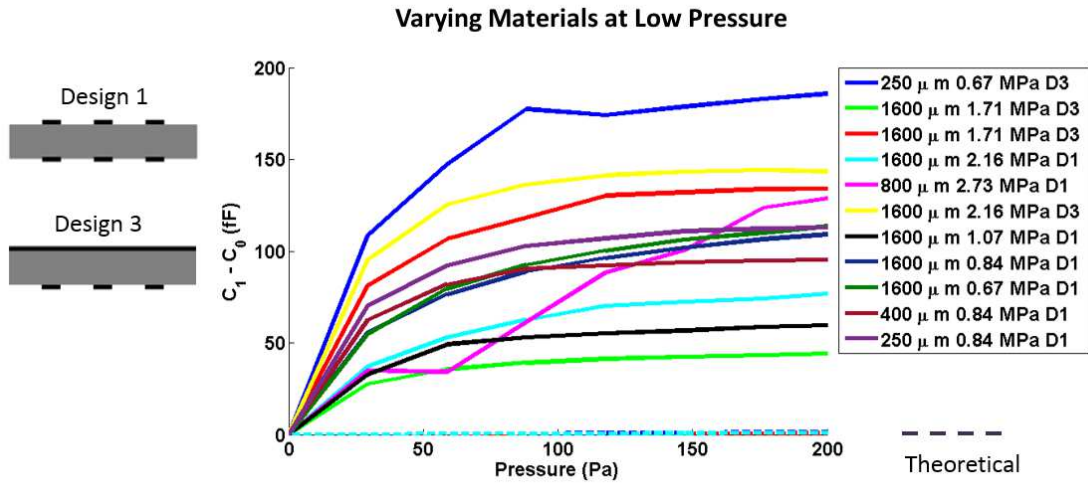
Figure 3.13: All materials tested at low pressures deviate from theoretical

two layers of PDMS, resulting in a total thickness of 2 mm. The embedded array was composed of a layer of PDMS that was first baked at 125°C for 1 hour, followed by placing the 0.843 MPa sensor sheet on top, pouring another layer of PDMS and

curing again at 125°C for 1 hour.
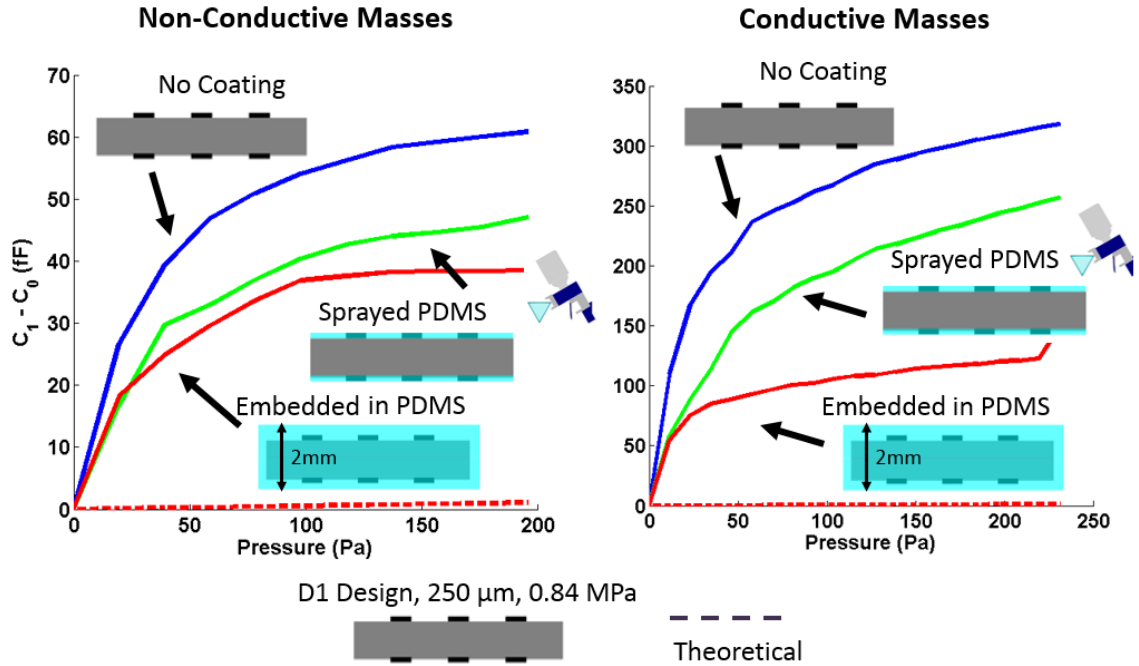
Figure 3.14: Arrays with no PDMS coating, sprayed-on PDMS, and embedded in PDMS at low pressures with conductive and non-conductive weights

When comparing the experimental data again to theoretical capacitance of a 0.843 MPa sheet, seen as dashed lines in Figure 3.14, the low pressures did not match. However, a noticeable difference is seen when comparing the stacked non-conductive Delrin squares, with dimensions of 1 x 1 x 0.24 cm each, and the stack of conductive silicon squares with dimensions of 1 x 1 x 0.05 cm each . As seen in Figure 3.14, all the materials had increased in capacitive measurements when conductive weights were measured, but the rate of increase was different for the materials at the same pressure. For instance, at 100 Pa, the embedded array increased from 35 fF to approximately 100 fF, about 3x greater. For the spray coated PDMS

42

sheet it increased from 40 fF to 180 fF at the same pressure, an increase of 4.5x. Finally, the non-coated sheet increased from 55 to 250 fF, an increase of approximately 5x. Due to the disparity in thicknesses of conductive and non-conductive materials, it is unclear if this may be a confounding factor in the results. While it may be possible that utilizing PDMS as a coating to reduce capacitive loads may be suitable for scenarios where conductive materials will be used, futher modeling and fabrication variation testing would be required to verify this.
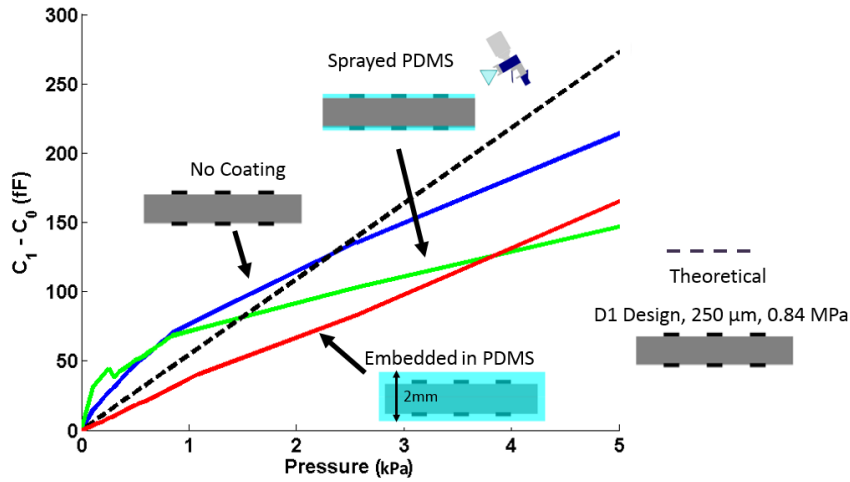
Figure 3.15: Arrays with no PDMS coating, sprayed-on PDMS, and embedded in PDMS at high pressures

High pressure testing for the uncoated, coated, and embedded arrays was limited to 50 kPa but had utilized the same test setup as identified in Section 3.1. As expected, the sprayed array and embedded array had increased in stiffness, though a theoretical model was not determined. While conductive shielding would likely prove suitable in preventing such electronic interference issues as seen in the works of [6] , the methods of fabrication towards such device turned out to be complex or

unsuitable. Either additional layers of PDMS and cPDMS would be sprayed on to create a shielding layer, or layers would be applied on of spun PDMS and cPDMS sheets, but issues of pad connection to the chip and delamination of layers rendered these methods inadequate in functionality or repeatability. However, it is essential that future sensor arrays have such functionality, and thus future iterations of this tactile system must address this issue.

Determining the ranges of forces the tactile sensors is essential in developing a proper assessment of suitable materials for a tactile system. While the testing apparatus was limited in its range of forces it was able to apply, the data obtained are still suitable for understanding the capacitive/force relationships in the force ranges needed for gentle touch and object manipulation [19]. Additionally, certain designs may be ruled out in future systems likely due to complicated geometries not considered in the parallel plate model. Further assessment of stacking sheets of differing moduli and thickness to obtain a greater dynamic range is currently being tested and may be added as an addendum to this work.

3.4   Dynamic Force Testing

Dynamic force testing is essential to understand the limitations of the sensing array. The capacitive sensing chip has an ingrained limitation for bandwidth testing, as its sampling rate is limited to 90.9 Hz, or 11ms. However, material testing can be a different concern, in that issues such as hysteresis and crack propagation may arise when cycling loads at high frequency [45, 46]. The testing apparatus as described

in Figure 3.1B utilized a motorized beam connected to a stepper motor which was controlled via an Arduino microcontroller. This provided low frequency testing and was limited to forces of approximately 3 kPa. In order to distribute the force a 300 mg 1 x 1cm Delrin square was placed ontop of the sensor being tested. When comparing the change in capacitance to a similar load on a D3 0.667 MPa array in Section 3.3 the forces match well to previous experimental data, i.e. a 10 gram load provides an additional capacitance change of approximately 50 fF. Materials were tested three times to determine a dynamic test profile. Material used in Figure 3.16 was a D3 0.667 MPa 255 μm sheet with a load cycled 10 times at 1.5 Hz. For most low pressures and low frequencies, the low modulus material responds well are returns back to a nominal value. However, at a pressure of 3000 Pa, indicating a 0.3 N force on the cm squared area, some hysteresis occurred. After approximately one second after beam liftoff, the capacitance reduced to a constant value of 4 fF. This was the highest hysteresis seen in both lower and higher pressures, and it is unclear if this was due to test apparatus limitations, or another issue not considered.

Dynamic Testing at Low Frequency
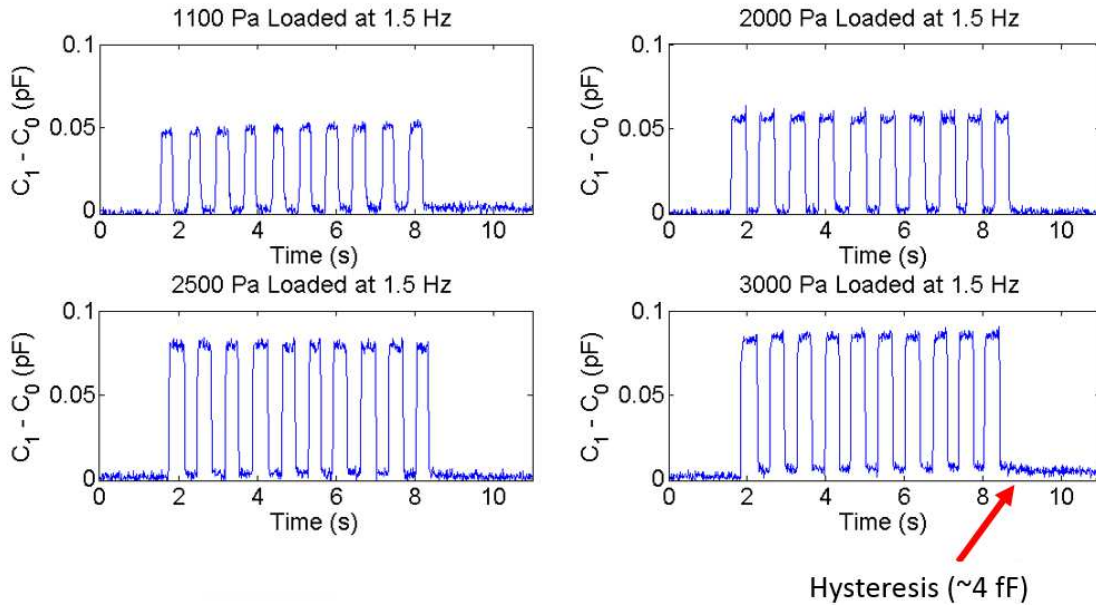
Figure 3.16: Sample of various bandwidth tests at low frequency on a
D3 0.667 MPa Sheet

The setup in 3.1B was enhanced with a DC motor controlled via an added motor shield to the Arduino microcontroller running at 5 volts. This allowed for higher frequency testing and higher loads. Material used in Figures 3.18 and 3.19 was a D1 0.843 MPa 381 μm sheet with a load cycled 100 times at 27-4.44 Hz. Due to limitations in the test setup, frequencies greater than 27 Hz were not obtainable. The load cell had an update rate of 6 ms, and measured a force of 1.2 Newtons (load of 120g) for all scenarios At 27 Hz the sensor consistently measures a reading of approximately 1.120g weight load, with hardly any hysteresis, <1 fF . An inset is shown in Figure 3.17, highlighting that the sensor does in fact read 27 separate cycles . When decreasing frequencies,seen in Figures 3.18 and 3.19, the sensor

array continued to match a capacitance readout of approximately 120g, with no hysteresis seen at 15 Hz. Further improvements in a testing apparatus may reveal the sensors are capable of measuring forces at higher frequencies, but are still limited by the AD7746 sensing chip, which has a limiting sampling rate of 90 Hz. Due to this sampling rate limit, suitable frequency testing would be limited to its Nyquist frequency of 45 Hz.
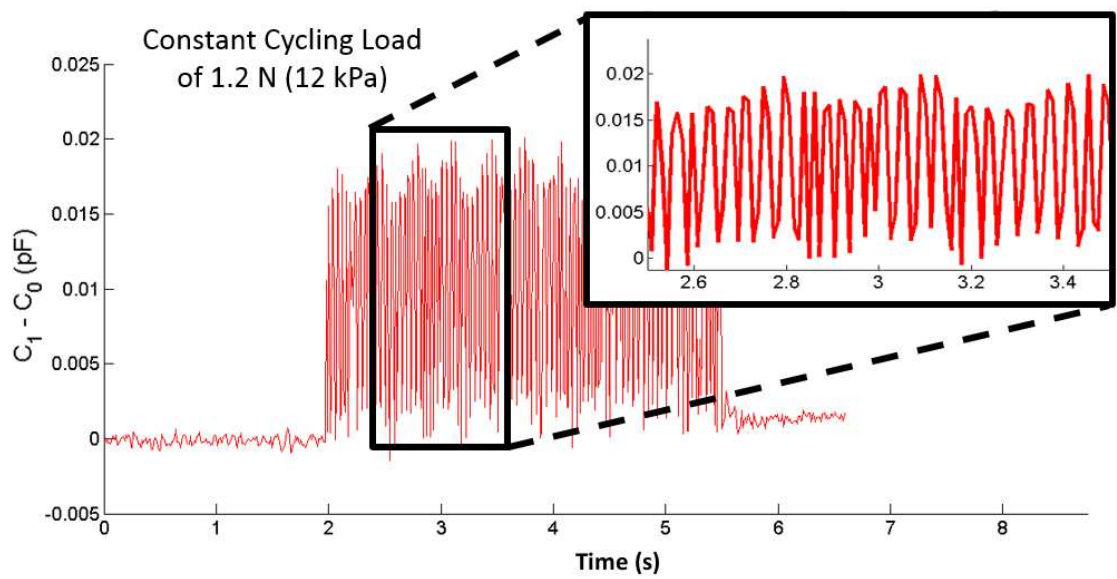
Figure 3.17: Sample of 12 kPa pressure test at 27 Hz frequency on a D1 0.843 MPa Array
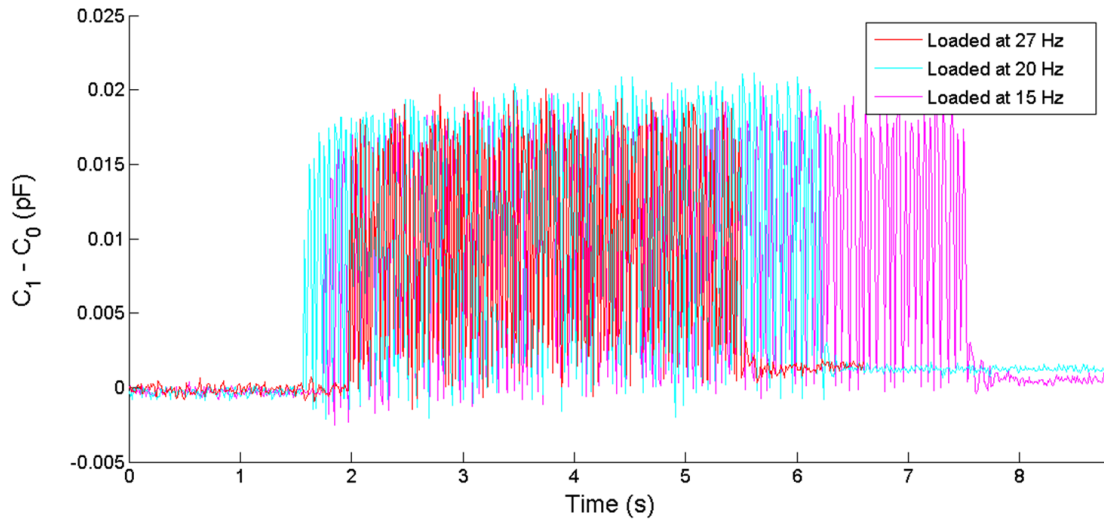
Figure 3.18: Sample of 12 kPa pressure test at high frequencies on a D1 0.843 MPa Array
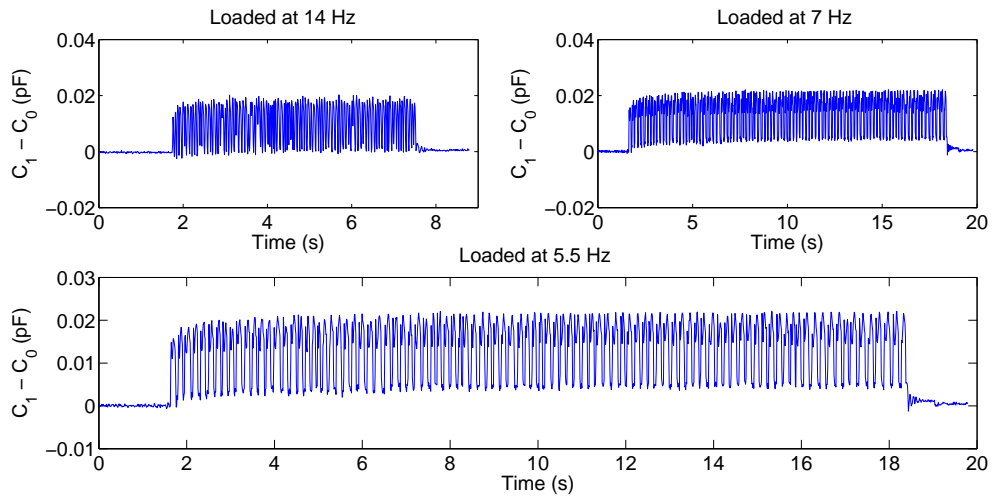
Figure 3.19: Sample of 12 kPa pressure tests at low frequencies on a D1 0.843 MPa Array

3.5   Abrasion Testing

An issue highlighted in [1] identifies an issue of sensor networks being exposed to corrosive or abrasive environments. Additional concerns are highlighted later in Chapter 4. This was therefore included in the requirements of the tactile sensing system and testing was performed for mechanical abrasion with and without exposure to solvents. The test designs are identified in Table 3.2 and detailed results are in Appendix C along with a sample of tested materials seen in Figure 3.21.
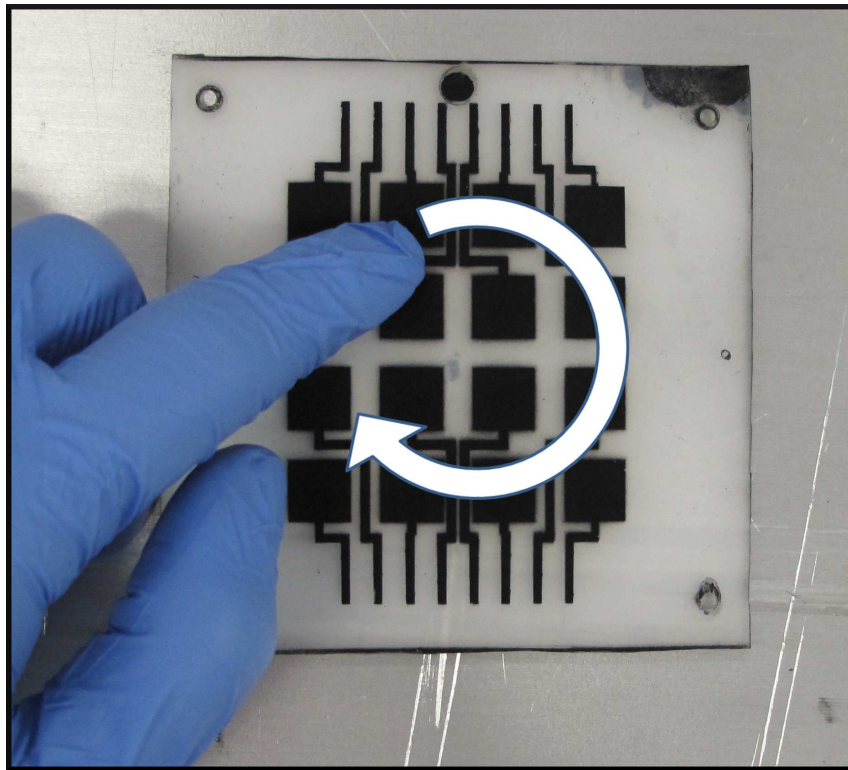
Figure 3.20: Visual demonstration of abrasion test

A sensor array is rubbed in a clockwise motion with a textured VWR MICROGRIP glove

Abrasion testing utilizing solvents removed the most material, likely due to

Figure 3.21: Sample set of materials from differing abrasion tests

Dry Abrasion	Sensor array rubbed in clockwise motion with textured VWR MICROGRIP glove
Wet Abrasion	Sensor array soaked with Solvent and rubbed in clockwise motion with Kimwipe

Table 3.2: Abrasion Test Definitions
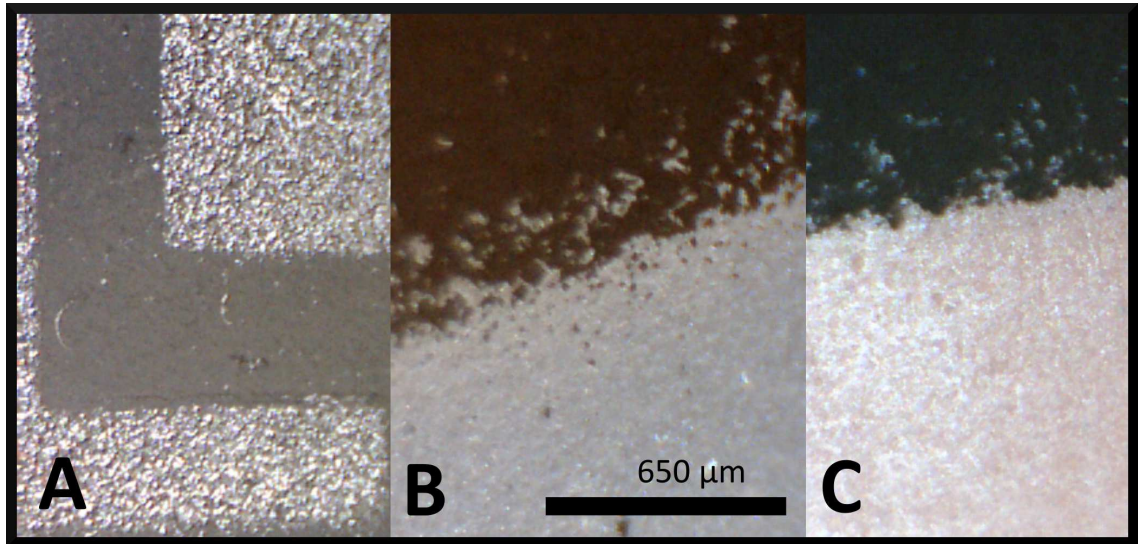
Figure 3.22: Rough and smooth textures of dielectric sheets viewed with 150x optical magnification

Materials reveal rough (A) and smooth (B,C) textures when magnified. All images are scaled to the 650 μ reference bar.

polymer swelling [47] and PDMS-PDMS delamination [48, 49] where non-crosslinked oligomers which can aid in adhesion [50] are extracted from PDMS and enter into the solution [48, 51, 47]. Additional results identify that surface roughness was the best indicator for longer lasting applications, and textures of materials can be seen in Figure 3.22, where grey 0.843 MPa 255 μm sheets (Figure 3.22A) have a rough characterstic in comparison to white 1.71 MPa 1600 μm and orange 2.16 MPa 1600 μm sheets seen in Figures 3.22B and C, respectively . Surface roughening has been

identified in literature for increased bonding strength [52, 53] as well as increased capacitance in microstructures [54], thus this would be an area to consider for further sensor array development.

3.6 Spatial Resolution Testing

As identified in Table 1.2, a key requirement for a tactile system is the capability to distinguish not only a force but a location of force relative to an orientation. Previous groups have utilized various grid arrays and encoders/decoders to determine location [13, 36, 23], however a similar setup with elastomer arrays proved unsuitable due to capacitive sensing chip limitations from serial resistance limits and capacitive sensing limits. Instead, sensor pads were connected via spray deposited cPDMS traces and were interfaced with a multiplexer/demultiplexer for the AD7746 chip to send and receive communication with each sensor pad. These pad locations were identified via their connection pin on the multiplexer, upon which the information was sent to a MATLAB program which visualized a change in capacitance, as discussed previously in Chapter 2, Section 2.1. Various sheets with differing design patterns, thicknesses and moduli were connected to an Arduino microcontroller via the custom-made ZIF-like connector as seen before and after assembly in Figure 3.1c and 3.1d and also seen in Figure 3.23. Data regarding comparisons of pressure profiles of an object on differing materials and thickness have not been collected at this time. Instead, designs were tested for pressure profile mapping. Certain designs such as D3 proved unsuitable for spatial resolution testing, as traces connecting to the sensor pad now
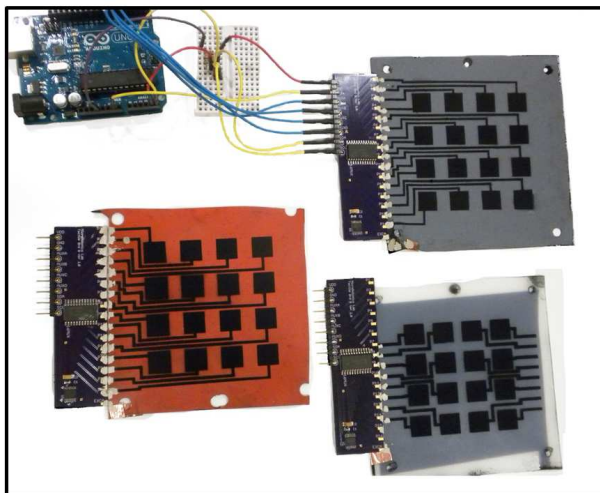
Figure 3.23: Examples of systems with custom circuit board and Arduino microprocessor connection with various substrates and design patterns

were extensions of the capacitor. This resulted in misidentification of location when an object pressed onto a trace. By varying trace designs on both the top and bottom of the sheet it is possible to reduce such misidentifications, and can be considered for future work.

As seen in Figure 3.25 , the sensor array is able to detect a pressure profile for both a plastic rollerblade wheel and a quarter on a D1 array. A noted issue for the quarter is that its conductivity results in a shorting of the taxels it is placed upon. Though it can clearly identify the location of the quarter, it is out of range of the capacitive sensing chip due to its conduction between taxels. PDMS coated arrays were investigated to identify if conductive materials would better represent its true mass, as seen in [6] and was reviewed in Section 3.3. However, spatial resolution profiling was not conducted with these coated arrays. Taxels on the arrays had been
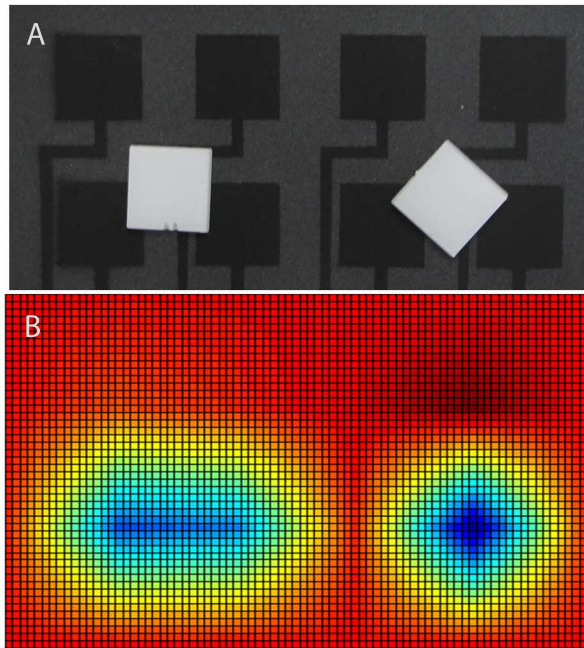
Figure 3.24: Approximations of object locations can be determined via visualization software. (MATLAB code adapted from [6])
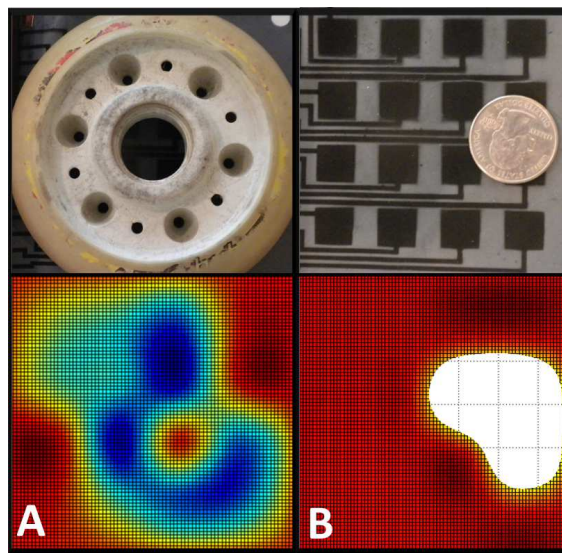
Figure 3.25: Nonconductive large wheel (A) and conductive quarter (B) on sensor arrays

tested to determine if they were functioning properly, but with extensive testing as traces and taxels can be worn and lose functionality, an area further discussed in the following chapter. As seen in Figure 3.25, it is likely that the lower lefthand taxel underneath the quarter failed, and thus the pressure profile for both the quarter and wheel do not reflect the pressure being recieved at this taxel.

3.7   Design Discussion

When considering the design of the sensor, each fabrication iteration provided its own benefits and limits. The first version (an alpha version not listed in this document) utilized aluminum foil as traces for the conductive elastomer pads which were spray deposited cPMDS on lab cured sheets of PDMS approximately 500 μm thick in a stacked sheet formation. These proved to be quite unwieldy, and had serious contact issues, where the traces often peeled off of the conductive elastomer contact after less than 3-4 weight load tests. The D3 arrays utilized the spray deposition of traces made of the cPMDS on and again was a stacked array. While the traces were now an integral part of the taxel element, developing a suitable contact to the capacitive sensing chip (AD7746) was still a formidable obstacle, where a use of headers and other metal probes was utilized to guarantee connection between the cPDMS layers and the excitation and capacitive reading channels of the AD7746. A third version (D1 in Figure 2.8) exchanged header connections for elastomer vias, and a double sided single sheet of capacitive arrays was now suitable. This allowed for the underside to have proper connections to the upper layer, and allowed for

connections to the sensing chip to be confined to only the top layer of the elastomer sheet. The vias had limitations as well though with extensive testing and fabrication yield. Due to the nature of the mixing process, a large amount of solvent was required to mix the proper amount of CB and PDMS to provide a suitable low resistance via that would be punched by a specialized hole punch. The curing process resulted in solvent evaporation and via shrinkage. This caused limited fabrication yield and limited testing repeatability due to vias breaking off or separating from the bottom layer traces from probe puncture or header connections.

Kovacs states that such circuits must also be integrated or positioned close to the actual sensors to reduce parasitic capacitance [42]. This was seen in experimentation of varied design patterns, where traces of extended length on a D3 sixteen patterned capacitor 0.667 MPa sheet, Figure 3.23, resulted in additional nontrivial capacitance(Figure 3.26) that made measurement of the whole array infeasible. The capacitive offset for this module was 16.87 pF, the maximum the chip natively can offset. Capacitances in parentheses are the upper/lower limits of the AD7746 sensing chip, which identify that these taxels are out of range for the chip to measure.

Testing of the highly compliant sensors revealed an interesting pattern: while low mass material (5 mg – 200 mg) would create a response in capacitance, the capacitance measured did not match theoretical calculations. However, a key issue was noted when completing these tests, where after a certain mass, approximately 1.4-1.7 grams , the capacitance was no longer as sensitive to small changes in pressure, and approached a quasi-linear relationship closer matching theory.

It was noted that with magnified visual inspection the sensor pads were slightly
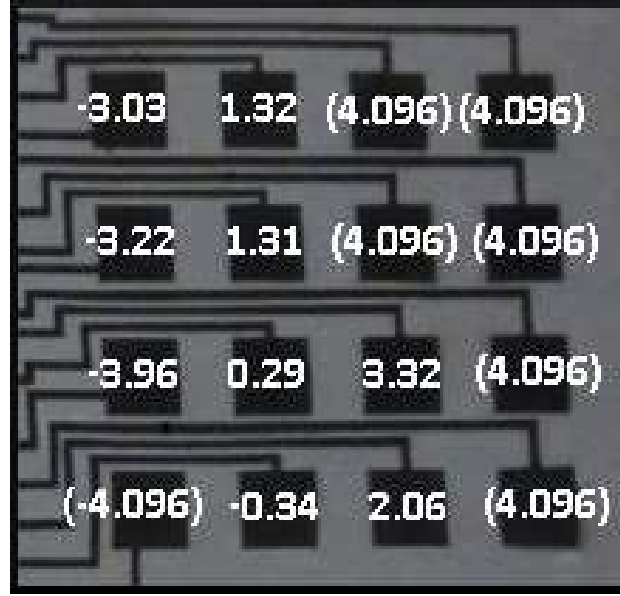
Figure 3.26: Design Pattern D3 with capacitances outside of sensing range

raised. A theory regarding this formation first considers the models done by Guth [55, 56] highlighting an increase in material stiffness with the CB filler, where a now a high modulus material ($\sim$6.7 MPa for bulk PDMS as identified by the Sylgard 184 datasheet) increases further in stiffness with added CB powder. Secondly, the solvent vehicle utilized during the spray deposition has been identified to cause PDMS swelling. Hexane, along with pentane, heptane, and an assortment of other solvents cause polymer swelling in PDMS [47] . With such a high mixture of hexane to PDMS, such a deposition would likely result in extensive swelling of the material. During curing process as the hexane evaporated the polymerization process resulted in a conformation to a "bubble" shape, where the cured high modulus material has conformed to the bump shape. The softer material substrate (Silicone HT6220, 0.846 MPa) conforms to this ridgid material and results in the bump artifact witnessed in

the array taxels. However, such an bump feature has proven beneficial, in that a the sensors have been determined to be highly sensitive, with a sensor resolution of 0.5 Pa. Once the bump has been deformed and flattened by adequate mass and setting this threshold capacitance as a baseline, the sensors reveal a repeatable response from 1 kPa up to approximately 120 kPa.

Chapter 4:   System Concerns & Applications

4.1   System Concerns (Verification and Validation in Sensor Networks)

An area of consideration for sensor networks is the determination of sensor providing the correct information. An issue for faulty sensors is that there is no suitable way to validate their information when considering a certain sensor in an array. There are multiple instances where an object can be on an array and result in a variation of sensor outputs. There is no clear way guarantee that one sensor is not functioning correctly, as there are a variety of differing pressures that may be applied, say via the point of an elbow, onto multiple sensors on a given area. If the same array had received pressure from a three-pronged actuator like in Figure 4.1 there would be no distinguishable difference in pressure profiles if a set of taxels was not functioning properly. Incorporating redundancy, i.e. a set of taxels would be utilized as duplicates for another set, in a sensor network would not be suitable as a means of verification or improved reliability without compromising spatial resolution. As seen in Table 4.2 a variety of concerns result when considering sensor networks. While a majority of these concerns are included in the requirements, a bigger issue

is determining the modes of failure with sensor networks and individual sensors. As seen in Table 4.1, there are a wide variety of failure modes and their causes that can occur, but when presented to the robot or other user of the system, there are instances of one failure effect, incorrect output, that results from all of these failure modes. It is imperative that the failure cause is determined so that the system can again operate nominally. A future goal would to identify a suitable power-on self test for each sensor. This could utilize the limitations of the capacitive sensing chip, where an absolute negative reading may be representative of a destroyed taxel or broken trace.

Additional concerns are the direct wear of the cPDMS over extensive testing. Contact points seen on extensively tested materials had shown noticeable wear patterns and an increase in resistance, identifying that conductive material was likely being removed. This conforms with the abrasive testing done earlier. As discussed in Section 3.5, ways to overcome this may be purchasing textured sheets or roughening the surface before spray deposition for greater adhesion.

4.2 Materials Review

When choosing a suitable conductive material it was essential that the material handle a certain number of criteria. Often the criteria came at a tradeoff, where the conductivity of a material was in direct relation to the cost. Silver particles provided high conductivity but had an issue with improperly mixing with the PDMS, where silver particles would settle to the bottom of a soultion in less than 30 seconds.
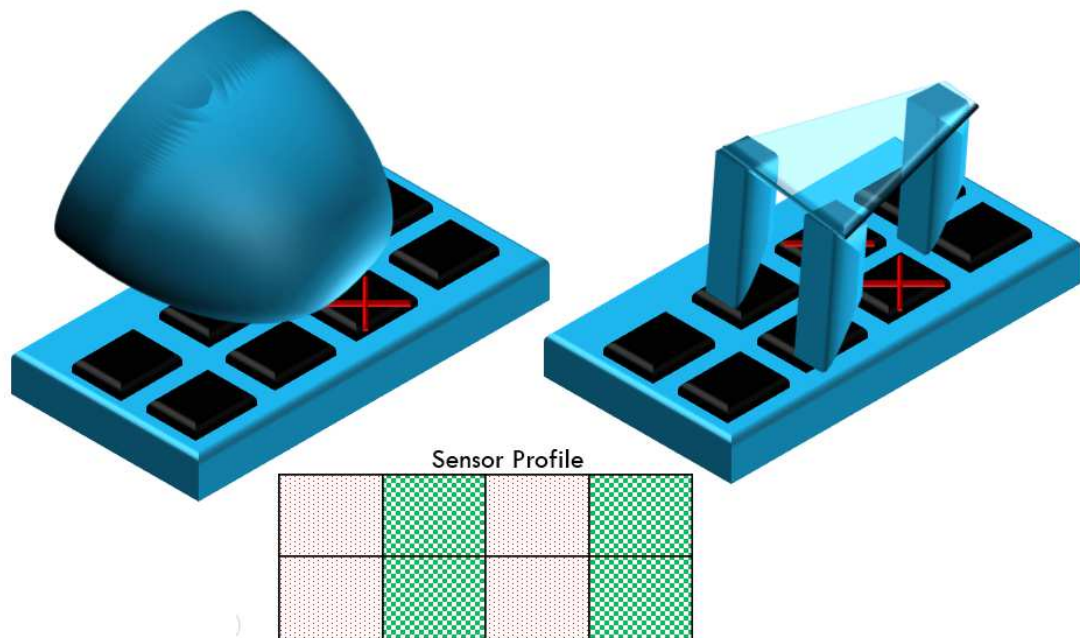
Figure 4.1: Indistinguishable Pressure Profiles when Taxels have Failed

CNTs and nanofibers were considered for investigation, but still the cost per gram of material would render the sensors too costly, even if weight percentages in a PDMS mixture were reduced to produce the minimum conductivity required. However, when utilizing carbon black, this too had its own issues. Due to the low density of the material, a large volume of carbon black was needed to obtain a given weight percentage. This required using a suitable vehicle that allowed for proper mixing of carbon black and PDMS. A ratio of 2:1 had previously been found to provide suitable mixing for carbon black (Alfa Aesar 50% compressed) at a 12.5% wt. ratio. This provided approximately a resistivity of 0.35 Ω -m .This was initially tested by mixing the material and then spin coating it at 1000 rpm. The material was cured and resistance was measured via a multimeter across cut squares of the material.

61

Failure Causes	Failure Modes	Failure Effects
Hardware error	Defect in D/A conversion	Incorrect output
Defect in A/D conversion, software error	Incorrect signal from sensor	Incorrect output
Software error	Conditioning of data from sensor is incorrect	Incorrect output
Software error	Corrupted signals to data processing or external system	Incorrect output
Failure of communication interface	Error on calibration	Incorrect output
Human/software error	Incorrect setting of parameters	Incorrect output
Hardware error	Loss of clock, wrong or changing frequency	Incorrect output
Wire failure	Loss of voltage to processor	Loss of signal history, calibration and settings information
Wire failure	Loss of voltage to sensor subsystem/ADC	Loss or incorrect measurement of input signal
Wire failure	Loss of voltage to human interface	No display of data, setting of parameters not possible

Table 4.1: A Selection of Failure Causes, Modes, and Effects of Sensors

The dimensions of the squares were measured via digital calipers and a resistivity was calculated. This resistivity proved to be too high for thin traces to and from the capacitive pads. As lower resistances were required in order to utilize the capabilities of the AD7746 chip, the CB % was increased to 17.5%, which was tested to have a resistivity of 0.16 Ω- m . However, when increasing the weight percentage, issues began to occur during the curing process. One of the more troubling issues was the severe cracking that formed during curing, rendering sheets of the material unusable. Another issue was the often inability for the material to fully cure. This may be due to a variety of factors not considered, such as incomplete mixing, or higher

Battery life, battery backup, uninterruptible power supply	Sensor positioning in target area	Sensor connectors & connections
Individual sensor failures redundant sensor connection	Number of sensor nodes in the network	Data routing efficiency
Average reading of multiple sensors	Data generation rate of sensor nodes	Sensor accuracy requirements
Energy consumption rate	Short and long term drift	Response timings requirement
Operating temperature	Corrosive environments	Protective layer/ Active protection

Table 4.2: Concerns for Sensor Networks (Adapted from [1])

temperatures and/or longer curing times were required. Another consideration was to run the material under vacuum to remove as much solvent as possible, but this often ended with material that did not fully cure or if vacuumed before spinning, did not spread evenly.

Chen et al. 2009 [53] have tested the bonding properties of PDMS and nano size (20-40 nm) CB, and were capable of obtaining mixtures up to 25% CB, (Alfa Aesar's CB particle size is an average of 42 nm) though it is noted that their mixing method varies from what has been utilized in this research, namely a 24 hour mixing of carbon black with the base material before the curing agent was added. However, by approaching the conductive material layering in a different manner, this problem was averted. By mixing at a high solvent ratio and spray depositing the conductive elastomer as seen in [57] the issue of cracking was solved at a macroscale, though still visible at the microscale as seen Figure 4.2 . Alternative conductive fillers should still be investigated, as long as they comply with the requirements of Table 1.2 . Exfoliated graphite has proven to be inexpensive, conductive and works well in
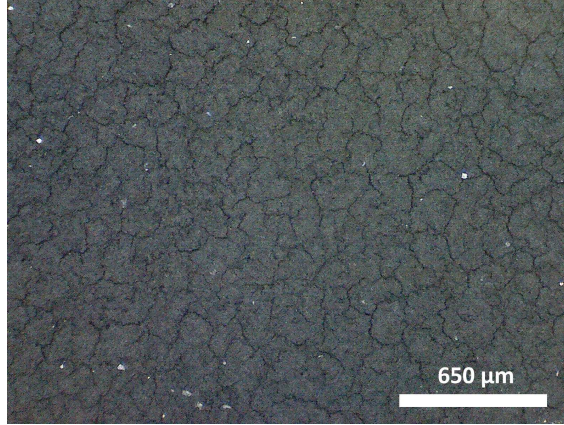
Figure 4.2: Small cracks can be seen in cPDMS sensor pad with 180x optical magnification

mixing with PDMS[58], and may be a possible alternative to the limitations of CB.

An area of interest when creating these sensor arrays is to make certain the materials utilized are compliant and flexible. As PDMS was chosen for its ease of purchase as well as previous testing done within the lab, it has shown some drawbacks during fabrication of the tactile systems. As noted in Table C.2, cPDMS did not adhere to certain substrate materials. These include Neoprene, natural rubber latex (NR), styrene-butadiene rubber (SBR), and surprisingly, silicone foam rubbers. To understand this problem, a literature review was done to better understand the possible polymer incompatibilities. A noted similarity between the rubbers, aside from the silicone foam, was found to be a key issue. Latex is also known as poly-*cis*-isoprene. Isoprene is 2-methyl-1,3-butadiene, i.e. butadiene with a methyl group attached. Neoprene is also known as polychloroprene, with the monomer being 2-chlorobuta-1,3-diene, so again another butadiene with a functional group. Polybutadiene (PBD) is immiscible with PDMS, and end groups are

64

used to increase adhesion between the two [59]. Neoprene, Isoprene (Natural Rubber Latex), and Styrene-Butadiene are all natively immiscible with PDMS and require additional functional groups for bonding/blending, [60, 61]. Even with functional group additions PDMS has been found to diffuse to surfaces from blends [61], while the adhesive interface is the most likely point of rupture or failure due to shear velocity or [62]. Interestingly, NR and SBR are immiscible with each other as well [61]. Even components of similar polarity and unsaturation can have cure imbalances if their crosslink reactivities are different, as has been observed in vulcanization and peroxide curing of NR/PBD blends [61].

An interesting case is the uncured cPDMS on silicone foam. It is unclear if the foam was treated with any materials, and inquiries for datasheets regarding the material have not been answered. As stated earlier, it may be possible that the curing agent was absorbed into the material, but it is still perplexing that previous textured silicone sheets provided suitable adhesion and curing. It may be possible to attempt other methods of PDMS-PDMS bonding, such as plasma bonding or corona discharge bonding. However research had found that simply using partially cured PDMS or uncured PDMS provided adequate bonding strength, while exceeding 250 kPa pressures at the interface of two PDMS layers before delamination, proving better bond strength than oxygen plasma bonding and corona discharge [52]. Thus the question towards the incompatibility of this silicone foam rubber and spray deposited cPDMS is still left unanswered.

What is most interesting is that the cPDMS on these sheets *have never cured.* As of this writing, sheets of latex sprayed with cPDMS three months ago are still un-

cured and smudge when touched. It is suspected that the curing agent for Sylgard 184, a proprietary platinum-based catalyst, is prevented from functioning or absorbed into the sheets. While PDMS has been investigated almost exclusively, other elastomers should not be ruled out. Water soluble latex and exfoliated graphite were spray deposited in [57], while MRTV-9 and CB at a similar weight

Matching the proper response for artificial skin also requires identification of proper musculature relationships and modeling of the skin. Proper modeling of the skin requires certain deformation testing, as seen in [63, 64], where Ogden as well Tong and Fung models for anisotropic responses in human skin were investigated. Such models may prove viable for elastomer skins as well, and while model fitting has been investigated recently for the D1 design, it has not been thoroughly reviewed for validation.

Lastly a key area of concern that this research was unable to address was the issue of sensor electronics integration. Interconnects are still required to connect the soft compliant silicone to the hard printed circuit boards containing the capacitive sensing components and microcontrollers. Groups such as [65] have investigated methods of improving interconnections between rigid and soft materials for electronics, though liquid metals in elastomer channels were used as the conductive connection. In order to scale these large area tactile arrays to the surface of a robot the electronics must be flexible as well, though it may be possible to include these components in a rigid polymer layer below, akin to the PCB/sensor layering of [6]. Another area of concern is information processing and interconnection, as well as power supply. Methods include inductive coils embedded into the skin

66

for both power and signal transmission of wireless sensors[66] as well as utilization of conductive rubber which sandwiches tactile sensors for power and bussed serial communication[67]. These methods may be investigated further for future design iterations.

4.3 Applications

Applications of the tactile array described in this thesis are numerous. Pritchard et al. provides a simple breakdown of possible applications and their required pressure ranges [2] of which all exept for in-shoe pressures has been demonstrated by this tactile array system.

Application	Pressure
Vascular pulse (75-150 mmHg)	10-20 kPa
Human fingertip texture, shape sensing	10-40 kPa
Hand grip	0-100 kPa
Fingerprint sensor	1-2 kPa
In-shoe pressures	< 1 MPa

Table 4.3: Possible applications and required pressure ranges (adapted from [2])

When considering the utility of such an array and its supporting electronics for podiatry-based applications, 90.9 Hz may be limited for uses in attempting to understand gait issues in humans via plantar pressure profiling, especially when testing human vibrational thresholds in feet (125 Hz) [68]. However, due to the high sensitivity of the sensors testing in the lab have shown possible opportunities in understanding gaits of harvestmen, also known as daddy long legs.

Considering other health monitoring and health service applications, the area of prosthetics can benefit from such large area pressure sensing systems. Such a sys-
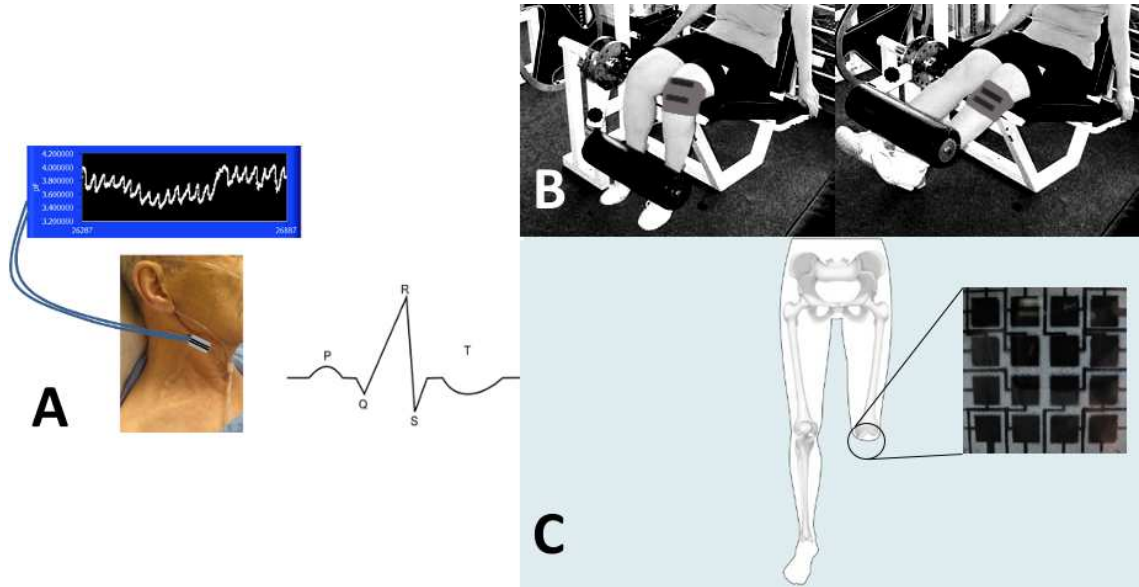
Figure 4.3: Assorted potential applications

tem could be utilized for haptic feedback or better understanding of where pressure hotspots are located and can be incorporated with neuromechanical functions. Additionally, the stretch and contraction of capacitors along joints can identify various flexion and extension of muscles for physical therapy training and range of movement, etc. as opposed to using goinometers which often require hold and measure methods [69]. This is often seen with strain gauges, and many groups are in pursuit for the consumer market [65, 70]. Lastly, as identified in Table 4.3, the vascular pulse of blood can be easily measured with elastomer capacitors, and recent testing has proven a heart rate is extractable from the capacitive signal seen in Figure 4.3.

Also consider also the applications for power-suits or trauma-preventive incidents. Given that the human bone ranges in strength as age varies, with the tibia having a yield strength of 120 MPa at age range 20-29 while gradually decreasing to

104 MPa at the 80-89 age range [71], it would be beneficial to not only measure such impacts but also be capable of providing a response mechanism to prevent fracture. An example would include a flexible cast-like material for older adults. This could be worn as a low profile elbow or knee pad or along the waist where on the outside the elastomer sensors would be placed. In combination with accelerometers the force sensors could be utilized in deploying an air-bag like system to prevent fracturing of bone during a fall, recording the incident and providing the data to a hospital for analysis of blunt force trauma. Such sensors would also be useful in crash test dummies to better understand the forces involved during air bag deployment. Other areas include instances of recording forces for training such as in pat down procedures in security. It is especially important for astronauts to determine proper forces that are being placed on their body, as extended flights have identified major bone loss due to bone demineralization [71]. Such response/feedback mechanisms can provide the understanding of forces that a foot or palm might feel when lifting weights or jogging with a weighted belt as well as testing gait patterns discussed in [68].

4.4 Conclusions

A simple approach to fabricating all elastomer capacitive tactile arrays was developed utilizing simple COTS elements and inexpensive materials. Purchased elastomer sheets were spray coated with cPDMS via a solvent vehicle and connected to low power capacitive sensing chips for force and location detection. Even at the

laboratory scale, the production of these sensor arrays was less than 12 cents per taxel. This fabrication may be done via roll to roll process, allowing for easy transition to industrial manufacturing and likely capable of dropping the manufacturing cost to fractions of a cent. Three design variations were investigated, two variations investigated double-sided sheets with conductive material spray deposited on both sides, while a third variation investigated single sided stacked sheets. The double sided designs included one variation with had sensors patterned on both sides of the sheet, D1, while the other variation utilized one patterned side and the opposing side being totally covered with cPDMS. A fabrication artifact was witnessed in the spray patterned sheets, where small bumps were formed, likely due to polymer swelling and conformation during the cure process. A variety of materials differing in thickness, modulus, and texture were investigated to determine the range of forces suitable for object grasping and light touch detection. Custom testing apparatuses were developed testing of static loads, dynamic loads, and spatial resolution testing. The experimental data for the force/capacitance relationship was compared against the theoretical capacitance of a flat plate capacitor model. The single sided stacked sheet design was tested on elastomer sheets with Young's modulus of 0.843 MPa and 255 μm thick and revealed a linear relationship at high loads, but deviated greatly from theory, likely due to complex geometries created during the fabrication process. Double-sided patterns deviated less from theory, and materials with higher modulus were found to match theory closer than low modulus materials. A linear relationship of force/capacitance was seen in all sheets tested in the range of 1 kPa to 120 kPa, within the desired range of forces for object manipulation. Materials

were highly sensitive to low pressures, capable of detecting less than 20 Pa, but als did not match well with theory, likely due to the fabrication artifact. Dynamic testing was performed at frequencies within the limit of the capacitive sensing chip (90 Hz), and showed no hysteresis at pressures of up to 12 kPa, limited only by the test setup. Spatial resolution of tactile modules showed reasonable profiles of objects placed on top of a sensor module, though conductive materials still prove to be challenging to accurately assess forces. Spatial resolution testing revealed an issue in the double-sided sheets with a fully sprayed underside of cPDMS, where traces to each sensor pad became extensions of the capacitor and resulted in misidentification of location when an object pressed onto a trace. Material compatibility of elastomers was reviewed, highlighting the incompatibility of PDMS with other elastomers. It is recommended that any further material choices are first investigated in literature to determine possible incompatibilities with other material or fabrication processes.

This project had considered aspects of material modeling, diagnostic testing, digital signal processing, and software/hardware verification. Requirements were developed and utilized in design and component decisions, and were useful for reference in testing apparatus development. Testing and possible failure identification were investigated, and future developments and concerns of sensor networks were discussed. Applications for the tactile arrays can include telerobotics and general robotic sensation enhancement, improved prosthetics functionality and body conformation testing, as well as health monitoring and physical therapy scenarios.

Further investigation of multilayered materials can be useful in improving the dynamic range or response of the sensor [72], though it is critical that there is

71

limited complexity in the traces/interconnections to keep fabrication and diagnostic of a failed taxel simple. Lastly, further integrating power supply and local processing will be useful in making certain such a device can be easily modularized for increased surface area coverage.

Chapter A: Arduino and MATLAB code

The Arduino programming environment and the varying hardware it supports was

utilized extensively in this research. Links to MATLAB and Arduino files can be

found at https://sites.google.com/site/microroboticslaboratory/projects/activeskins

.

Chapter B: Custom Circuit Board and EAGLECAD

A custom PCB was created via EAGLECAD to allow for testing of the modular tactile arrays. The board was designed to have as low a profile as possible while providing adequate trace thicknesses, gaps between traces and minimal number of vias. The dimensions of the board are 85.09 x 24.13 mm (3.35 x .95 inches) and exposed pads P1 through EXCA are .508 mm (0.2 inches) apart from their centers. A diagram of the board schematic is outlined below, followed by the board layout, and finally PCB manufacturer's printout design and completed board. Links to EAGLECAD files can be found at

https://sites.google.com/site/microroboticslaboratory/projects/activeskins

The parts list for the materials on the board are as follows:

Item	Mfr. Part #	Pkg. Outline
AD7746 Cap. to Digital Converter	AD7746ARUZ	16 TSSOP
16 Channel Multiplexer/ Demultiplexer	74HC(T)4067	24 SOIC
Tantalum Capacitor 10 μF	T491A106K010AT7280	1206 SMT
Ceramic Capacitor 0.1 μF	CL10B104KA8NNNC	0603 SMT

Table B.1: Components of custom PCB

Figure B.1: EAGLECAD Board Schematic
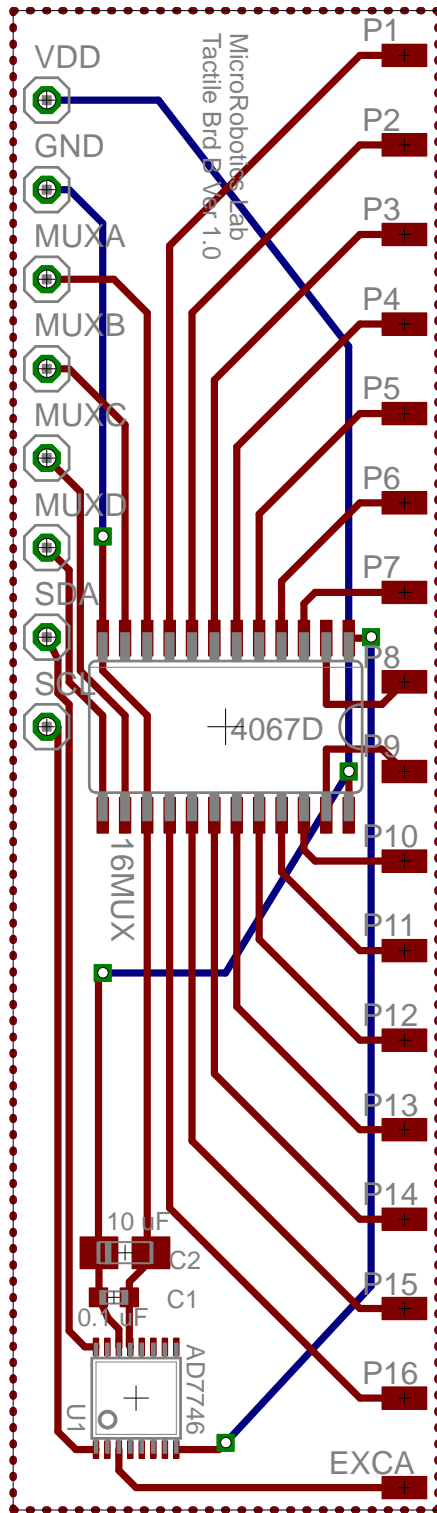
Figure B.2: EAGLECAD Board Layout

Upper layer traces are seen in red while lower layer traces are blue. Vias are seen in green.

76
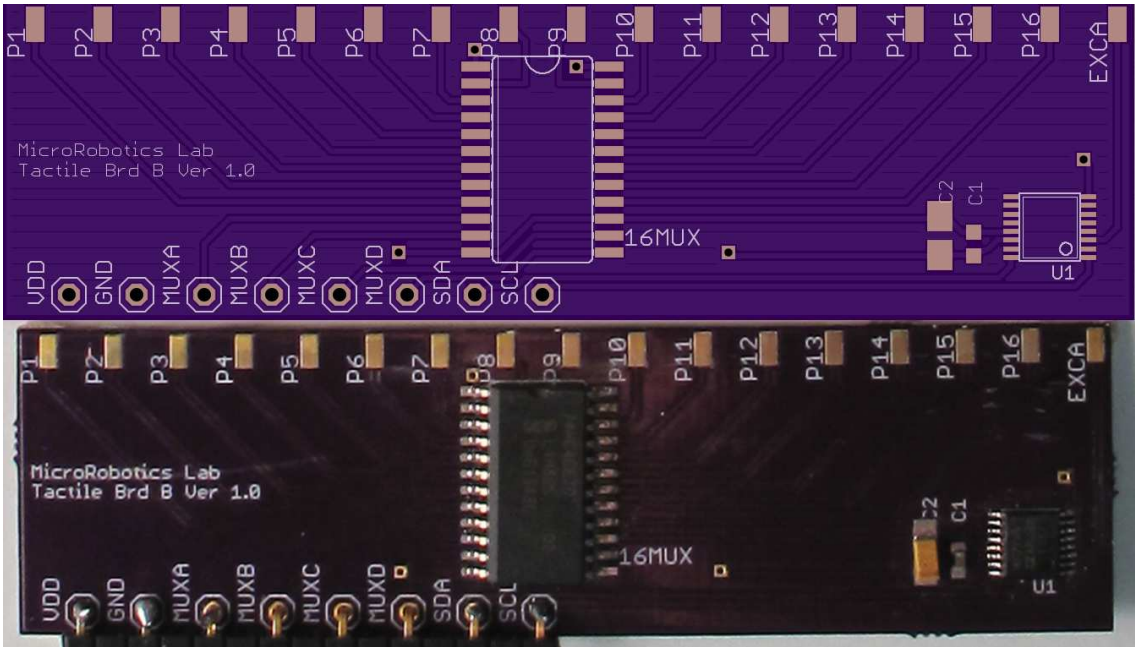
Figure B.3: Final design and assembled board

OSH Park's expected printed design and fully assembled board.

Chapter C: Material Supplier Identification, Abrasion Test Results and Cost Example

On the following pages are the material part identifications and cost estimates per sensor. The materials table identifes Amazon Small Parts and McMasterCarr as the main supplier, though the exact materials may be purchased from other wholesale suppilers or from the original manufacturer. Following this table is a simple cost calculation for fabricating the array of sensors. The estimate is based off of available materials as outlined below. A final table in this appendix provides the observed results from the abrasion test as outlined in Section 3.5.

Material	Backing	Texture	Thickness μm (mil)	Hardness Shore A	Young's Modulus (MPa)	Supplier	Part No.
Silicone (grey)	none	slightly mottled	254 (10)	10A	0.667	ASP	HT6210.0101212
Silicone (black)	none	slightly mottled	254 (10)	20A	0.843	ASP	HT6220.0101212
Silicone (black)	none	slightly mottled	381 (15)	20A	0.843	ASP	HT6220.0151212
Silicone (orange)	adhesive backing	smooth	794 (31.25)	10A	0.667	MMC	9010K41 Adhesive Back 10A
Silicone (orange)	adhesive backing	smooth	794 (31.25)	20A	0.843	MMC	9010K41 Adhesive Back 20A
Silicone (orange)	adhesive backing	smooth	794 (31.25)	30A	1.07	MMC	9010K41 Adhesive Back 30A
Silicone (white)	none	smooth	1588 (62.5)	50A	1.71	ASP	SILTRU-062I12I12I50A
Silicone (orange)	none	smooth	794 (62.5)	60A	2.16	MMC	8632K42
Silicone (orange)	none	smooth	794 (31.25)	70A	2.73	ASP	SRR70-0031-E
Foam Rubber (orange)	none	dense diamond	1575 (62)	N/A	(0.621-0.896)*	ASP	MC1135F-063X2411
Latex Natural Rubber (tranluscent yellow)	none	smooth	381 (15)	30A	1.07	ASP	SLR-020-E
Neoprene Rubber (black)	none	smooth	1588 (62.5)	60A	2.16	ASP	NP60S-0062-F
Styrene-Butadiene Rubber (red)	none	smooth	1588 (62.5)	75A	3.07	ASP	SBRS-0062-F

Table C.1: Materials and part numbers utilized in this thesis.

* Material listed as medium-firm, both medium and firm having differing moduli

Item	Amount	Unit	SKU/Description	Supplier	Cost ($)	Item Multiplier	Subtotal	Amount per batch	Unit	# of Batches Possible
Sylgard 184 kit	500	g	184 SIL ELAST KIT 0.5KG	Ellsworth Adhesives	46.1	1	46.1	16.5	g	30
Carbon Black, 50% compressed	250	g	39724	Alfa Aesar	42.6	1	42.6	3.5	g	71
Elastomer Sheet	9	ft^2	HT6220.0103636	Amazon Small Parts	96	3	288	0.89	ft^2	30
Hexane	1316	g	H302-4	Fischer Scientific via. UMD Chem Stores	36.24	2	72.48	80	g	32
Total Costs of all purchased materials ($)										**449.18**
Arrays per batch										**8**
Sensors per array										**16**
Sensors per batch										**128**
Batches via limited material										**30**
Total cost/ sensor ($)										**0.117**

Table C.2: Pricing cost example for batches of sensors produced

Modulus (MPa)	Thickness (μm)	Finish	Color	Dry Abrasion	Wet Abrasion I: Ethyl Alcohol	Wet Abrasion II: Hexane
0.667	250, 400	Slightly Mottled	Grey	No difference in appearance	Little to no removal of material	Light material removal around pad edges, all pads and traces still viable
0.843	250, 400	Slightly Mottled	Black	No difference in appearance	Little to no removal of material	Light material removal around pad edges, all pads and traces still viable
1.71	1600	Smooth	White	Moderate removal of material, pads have material missing, traces incomplete	Whole material removed, no cPDMS left	Almost all traces and pads removed
2.16	1600	Smooth	Orange	Light material removal around pad edges, all pads and traces still viable	Traces fully removed, pads show moderate material removal	Traces and pads have significant material removal, some traces fully removed

Table C.3: Abrasion Test

Chapter D: Sigma Delta Conversion Overview

A brief overview of Sigma Delta conversion is provided below. A simple interactive tutorial can also be found at:

http://designtools.analog.com/dt/sdtutorial/ADCTutorial.jar

A voltage to digital converter is seen in Figure D.1a. The sampling capacitor is charged during the first clock cycle (Figure D.1b) to V_{in}, and during the descent of the clock the charge from the capacitor is transferred to the integrator capacitor, C_{int}. This increases the integrator output voltage to $C_s V_i n / C_i nt$. While the output is negative, assuming $V_{ref} > V_{in}$, this process will repeat. The ratio of number of ones to the total number of clock cycles is equal to the ratio of $\frac{V_{int}}{V_{ref}}$. Comparatively, looking at a capacitive to digital converter (Figure D.1c) a reference capacitor is utilized but almost all the other components stay the same. Stated simply enough by Heidary "When the comparator output is zero (low), the charge of $C_x V_{ref}$ is transferred to C_{int} , and when the comparator output is one (high), the charge $(C_x - C_{ref}) V_{ref}$ is transferred to C_{int}" [7]. Again due to charge balancing at the integrator input, the ratio of ones to the total number of clock cycles is equal to the ratio of $\frac{C_x}{C_{ref}}$
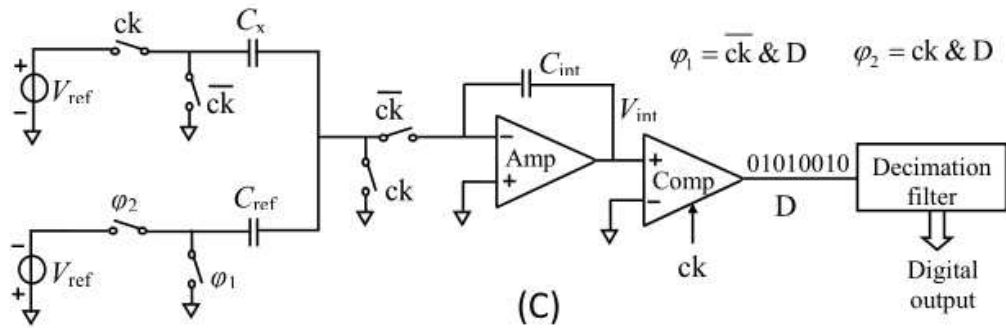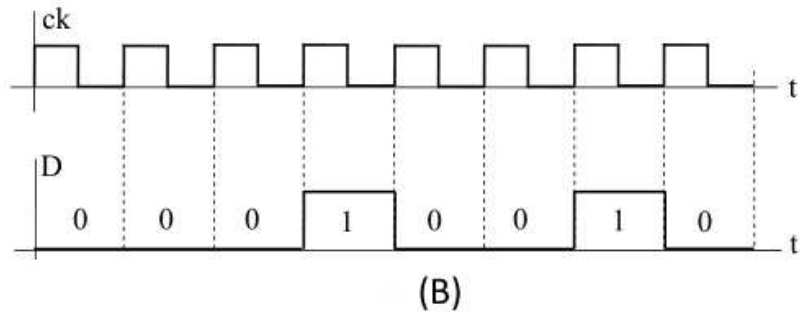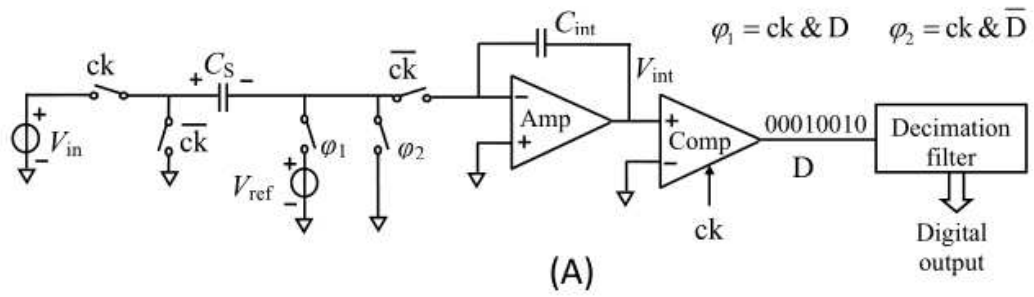
$\varphi_1 = \text{ck \& D} \qquad \varphi_2 = \text{ck \& } \overline{\text{D}}$

(A)

(B)

$\varphi_1 = \overline{\text{ck}} \text{ \& D} \qquad \varphi_2 = \text{ck \& D}$

(C)

Figure D.1: Sigma Delta Conversion (adapted from [7])

Bibliography

[1] NAVAL SURFACE WARFARE CENTER CARDEROCK DIV. Handbook of reliability prediction procedures for mechanical equipment. 1992.

[2] Emily Pritchard, Mohamed Mahfouz, B Evans, Sazia Eliza, and Mohammad Haider. Flexible capacitive sensors for high resolution pressure measurement. In *Sensors, 2008 IEEE*, pages 1484–1487. IEEE, 2008. doi:10.1109/ICSENS.2008.4716726.

[3] Tekscan. Inc. Grip force and pressure measurement system grip system for r&d tactile grip force and pressure measurement. [2014]. http://www.tekscan.com/grip-pressure-measurement.

[4] Takktile Inc. Takkarray. [2014]. http://www.takktile.com/product:takkarray.

[5] Peter D Block and Sarah Bergbreiter. Large area all-elastomer capacitive tactile arrays. In *Sensors, 2013 IEEE*, pages 1–4. IEEE, 2013. doi:10.1109/ICSENS.2013.6688345.

[6] John Ulmen and Mark Cutkosky. A robust, low-cost and low-noise artificial skin for human-friendly robots. In *Robotics and Automation (ICRA), 2010 IEEE International Conference on*, pages 4836–4841. IEEE, 2010. doi:10.1109/ROBOT.2010.5509295.

[7] Ali Heidary. A low-cost universal integrated interface for capacitive sensors, 2010. http://repository.tudelft.nl/assets/uuid:e2234250-950d-4eb5-9f2e-b5b8e67af2e5/Ali-Thesis.pdf.

[8] R.S. Dahiya, G. Metta, M. Valle, and G. Sandini. Tactile sensing–from humans to humanoids. *IEEE Transactions on Robotics*, 26:1–20, February 2010. doi:10.1109/TRO.2009.2033627.

[9] Howard R. Nicholls and Mark H. Lee. A survey of robot tactile sensing technology. *The International Journal of Robotics Research*, 8(3):3–30, 1989. doi:10.1177/027836498900800301.

[10] Hanna Yousef, Mehdi Boukallel, and Kaspar Althoefer. Tactile sensing for dexterous in-hand manipulation in roboticsa review. *Sensors and Actuators A: physical*, 167(2):171–187, 2011. doi:10.1016/j.sna.2011.02.038.

[11] Alan H Redford and Eddie K Lo. *Robots in assembly*. John Wiley & Sons, Inc., 1986. ISBN:0470203269.

[12] S. Cruz, N.J. Vieira, J.C. Viana, and L.A. Rocha. Low cost pressure mapping platform for mobility monitoring applications. In *Instrumentation and Measurement Technology Conference (I2MTC), 2013 IEEE International*, pages 967–970, May 2013. doi:10.1109/I2MTC.2013.6555559.

[13] Kunnyun Kim, Kang Ryeol Lee, Won Hyo Kim, Kwang-Bum Park, Tae-Hyung Kim, Jin-Sang Kim, and James Jungho Pak. Polymer-based flexible tactile sensor up to 32 x 32 arrays integrated with interconnection terminals. *Sensors and Actuators A: Physical*, 156(2):284 – 291, 2009. doi:10.1016/j.sna.2009.08.015.

[14] Yong-Lae Park, Bor-Rong Chen, and R. J. Wood. Design and fabrication of soft artificial skin using embedded microchannels and liquid conductors. *IEEE Sensors Journal*, 12(8):2711–2718, August 2012. doi:10.1109/JSEN.2012.2200790.

[15] Y-J Yang, M-Y Cheng, W-Y Chang, L-C Tsao, S-A Yang, W-P Shih, F-Y Chang, S-H Chang, and K-C Fan. An integrated flexible temperature and tactile sensing array using pi-copper films. *Sensors and Actuators A: Physical*, 143(1):143–153, 2008. doi:10.1016/j.sna.2007.10.077.

[16] Darryl PJ Cotton, Ingrid M Graz, and Stephanie P Lacour. A multifunctional capacitive sensor for stretchable electronic skins. *Sensors Journal, IEEE*, 9(12):2008–2009, 2009. doi:10.1109/JSEN.2009.2030709.

[17] Weili Hu, Xiaofan Niu, Ran Zhao, and Qibing Pei. Elastomeric transparent capacitive sensors based on an interpenetrating composite of silver nanowires and polyurethane. *Applied Physics Letters*, 102(8):083303, 2013. doi:10.1063/1.4794143.

[18] Darren J Lipomi, Michael Vosgueritchian, Benjamin CK Tee, Sondra L Hellstrom, Jennifer A Lee, Courtney H Fox, and Zhenan Bao. Skin-like pressure and strain sensors based on transparent elastic films of carbon nanotubes. *Nature nanotechnology*, 6(12):788–792, 2011. doi:10.1038/nnano.2011.184.

[19] Stefan CB Mannsfeld, Benjamin CK Tee, Randall M Stoltenberg, Christopher V HH Chen, Soumendra Barman, Beinn VO Muir, Anatoliy N Sokolov, Colin Reese, and Zhenan Bao. Highly sensitive flexible pressure sensors with microstructured rubber dielectric layers. *Nature materials*, 9(10):859–864, 2010. doi:10.1038/nmat2834.

[20] Ji-Eun Han, Dongil Kim, and Kwang-Seok Yun. All-polymer hair structure with embedded three-dimensional piezoresistive force sensors. *Sensors and Actuators A: Physical*, 188:89–94, 2012. doi:10.1016/j.sna.2012.03.045.

[21] Thomas V Papakostas, Julian Lima, and Mark Lowe. A large area force sensor for smart skin applications. In *Sensors, 2002. Proceedings of IEEE*, volume 2, pages 1620–1624. IEEE, 2002. doi:10.1109/ICSENS.2002.1037366.

[22] Tibor L Foldvari and Kurt S Lion. Capacitive transducers(capacitive transducers, their operation principles, design characteristics and physical properties). *Instruments and Control Systems*, 37:77–85, 1964.

[23] Hyung-Kew Lee, Jaehoon Chung, Sun-Il Chang, and Euisik Yoon. Normal and shear force measurement using a flexible polymer tactile sensor with embedded multiple capacitors. *Microelectromechanical Systems, Journal of*, 17(4):934–942, 2008. doi:10.1109/JMEMS.2008.921727.

[24] ChiaHua Ho, Wang-Shen Su, Chih-Fan Hu, Chia-Min Lin, Weileun Fang, and Fu-Liang Yang. A flexible, highly-sensitive, and easily-fabricated carbon-nanotubes tactile sensor on polymer substrate. In *Solid-State and Integrated Circuit Technology (ICSICT), 2010 10th IEEE International Conference on*, pages 1388–1391, Nov 2010. doi:10.1109/ICSICT.2010.5667624.

[25] Le Cai, Li Song, Pingshan Luan, Qiang Zhang, Nan Zhang, Qingqing Gao, Duan Zhao, Xiao Zhang, Min Tu, Feng Yang, et al. Super-stretchable, transparent carbon nanotube-based capacitive strain sensors for human motion detection. *Scientific reports*, 3, 2013. doi:10.1038/srep03048.

[26] Qing Cao and John A. Rogers. Ultrathin films of single-walled carbon nanotubes for electronics and sensors: A review of fundamental and applied aspects. *Advanced Materials*, 21(1):29–53, January 2009. doi:10.1002/adma.200801995.

[27] XZ Niu, SL Peng, LY Liu, WJ Wen, and Ping Sheng. Characterizing and patterning of pdms-based conducting composites. *Advanced Materials*, 19(18):2682–2686, 2007. doi: 10.1002/adma.200602515.

[28] Ganna Pugach, Viacheslav Khomenko, Artem Melnyk, Alexandre Pitti, Patrick Henaff, and Philippe Gaussier. Electronic hardware design of a low cost tactile sensor device for physical human-robot interactions. In *Electronics and Nanotechnology (ELNANO), 2013 IEEE XXXIII International Scientific Conference*, pages 445–449. IEEE, 2013. doi:10.1109/ELNANO.2013.6552033.

[29] Lisa Skedung, Martin Arvidsson, Jun Young Chung, Christopher M Stafford, Birgitta Berglund, and Mark W Rutland. Feeling small: Exploring the tactile perception limits. *Scientific reports*, 3, 2013. doi:10.1038/srep02617.

[30] Pauwel Goethals. Tactile feedback for robot assisted minimally invasive surgery: an overview. *Department of Mechanical Engineering KU Leuven, Tech. Rep*, 2008. https://www.mech.kuleuven.be/en/pma/research/ras/rasdocuments/Internal-Report-08RP012.pdf.

[31] Takayuki Hoshi and Hiroyuki Shinoda. Robot skin based on touch-area-sensitive tactile element. In *Robotics and Automation, 2006. ICRA 2006. Proceedings 2006 IEEE International Conference on*, pages 3463–3468. IEEE, 2006. doi:10.1109/ROBOT.2006.1642231.

[32] Michael SA Graziano. Where is my arm? the relative role of vision and proprioception in the neuronal representation of limb position. *Proceedings of the National Academy of Sciences*, 96(18):10418–10421, 1999. doi:10.1073/pnas.96.18.10418.

[33] S. Adee. The revolution will be prosthetized. *Spectrum, IEEE*, 46(1):44–48, Jan 2009. doi:10.1109/MSPEC.2009.4734314.

[34] L Martinelli, C Hurschler, and D Rosenbaum. Comparison of capacitive versus resistive joint contact stress sensors. *Clinical orthopaedics and related research*, 447:214–220, 2006. doi:10.1097/01.blo.0000218730.59838.6a.

[35] Jill M Brimacombe, David R Wilson, Antony J Hodgson, Karen C Ho, and Carolyn Anglin. Effect of calibration method on tekscan sensor accuracy. *Journal of biomechanical engineering*, 131(3):034503, 2009. doi:10.1115/1.3005165.

[36] Hyung-Kew Lee, Sun-Il Chang, and Euisik Yoon. A flexible polymer tactile sensor: fabrication and modular expandability for large area deployment. *Microelectromechanical Systems, Journal of*, 15(6):1681–1686, 2006. doi:10.1109/JMEMS.2006.886021.

[37] Mark H Lee and Howard R Nicholls. Review article tactile sensing for mechatronicsa state of the art survey. *Mechatronics*, 9(1):1–31, 1999. doi:10.1016/S0957-4158(98)00045-2.

[38] AN Gent. On the relation between indentation hardness and young's modulus. *Rubber Chemistry and Technology*, 31(4):896–906, 1958. doi:http://dx.doi.org/10.5254/1.3542351.

[39] Iranthi M. Meththananda, Sandra Parker, Mangala P. Patel, and Michael Braden. The relationship between shore hardness of elastomeric dental materials and young's modulus. *Dental Materials*, 25(8):956 – 959, 2009. doi:http://dx.doi.org/10.1016/j.dental.2009.02.001.

[40] Adel Siddiqui, Michael Braden, Mangala P. Patel, and Sandra Parker. An experimental and theoretical study of the effect of sample thickness on the shore hardness of elastomers. *Dental Materials*, 26(6):560 – 564, 2010. doi:http://dx.doi.org/10.1016/j.dental.2010.02.004.

[41] HJ Qi, K Joyce, and MC Boyce. Durometer hardness and the stress-strain behavior of elastomeric materials. *Rubber chemistry and technology*, 76(2):419–435, 2003. doi: http://dx.doi.org/10.5254/1.3547752.

[42] Gregory TA Kovacs. *Micromachined transducers sourcebook*. WCB/McGraw-Hill New York, 1998.

[43] Analog Devices. Inc., 24-bit capacitance-to-digital converter with temperature sensor, ad 7745/ad7746. 2009-08-24]. http://www. analog, com/zh/analog-to-digital-converters/capacitance-to-digital-converters/ad7745/products/product. html.

[44] Marvin H Cheng, GT-C Chiu, and Matthew A Franchek. Real-time measurement of eccentric motion with low-cost capacitive sensor. *Mechatronics, IEEE/ASME Transactions on*, 18(3):990–997, 2013. doi:10.1109/TMECH.2012.2195323.

[45] W.V. Mars and A. Fatemi. A literature survey on fatigue analysis approaches for rubber. *International Journal of Fatigue*, 24(9):949 – 961, 2002. doi:10.1016/S0142-1123(02)00008-7.

[46] A. Dorfmann and R.W. Ogden. A pseudo-elastic model for loading, partial unloading and reloading of particle-reinforced rubber. *International Journal of Solids and Structures*, 40(11):2699 – 2714, 2003. doi:10.1016/S0020-7683(03)00089-1.

[47] Jessamine Ng Lee, Cheolmin Park, and George M Whitesides. Solvent compatibility of poly (dimethylsiloxane)-based microfluidic devices. *Analytical chemistry*, 75(23):6544–6554, 2003. doi:10.1021/ac0346712.

[48] Kai-Seng Koh, Jitkai Chin, Joanna Chia, and Choon-Lai Chiang. Quantitative studies on pdms-pdms interface bonding with piranha solution and its swelling effect. *Micromachines*, 3(2):427–441, 2012. doi:10.3390/mi3020427.

[49] Bo-Yeol Kim, Lan-Young Hong, Young-Min Chung, Dong-Pyo Kim, and Chang-Soo Lee. Solvent-resistant pdms microfluidic devices with hybrid inorganic/organic polymer coatings. *Advanced Functional Materials*, 19(23):3796–3803, 2009. doi:10.1002/adfm.200901024.

[50] Elmar Kroner, Roya Maboudian, and Eduard Arzt. Adhesion characteristics of pdms surfaces during repeated pull-off force measurements. *Advanced Engineering Materials*, 12(5):398–404, 2010. doi:10.1002/adem.201000090.

[51] Zeyad Almutairi, Carolyn L Ren, and Leonardo Simon. Evaluation of polydimethylsiloxane (pdms) surface modification approaches for microfluidic applications. *Colloids and Surfaces A: Physicochemical and Engineering Aspects*, 415:406–412, 2012. doi:10.1016/j.colsurfa.2012.10.008.

[52] Mark A Eddings, Michael A Johnson, and Bruce K Gale. Determining the optimal pdms-pdms bonding technique for microfluidic devices. *Journal of Micromechanics and Microengineering*, 18(6):067001, 2008. doi:10.1088/0960-1317/18/6/067001.

[53] Hao Chen, Ionel Botef, Babu Guduri, and S Vallabhapurapu. Thermal and bonding properties of nano size carbon black filled pdms. 2009. URI: http://hdl.handle.net/10204/4514.

[54] Kenichi Takahata and Yogesh B Gianchandani. A micromachined capacitive pressure sensor using a cavity-less structure with bulk-metal/elastomer layers and its wireless telemetry application. *Sensors*, 8(4):2317–2330, 2008. doi:10.3390/s8042317.

[55] Eugene Guth. Theory of filler reinforcement. *Journal of applied physics*, 16(1):20–25, 2004. doi:10.1063/1.1707495.

[56] Robert A Shanks et al. General purpose elastomers: Structure, chemistry, physics and performance. In *Advances in Elastomers I*, pages 11–45. Springer, 2013. doi:10.1007/978-3-642-20925-3_2.

[57] James Wissman, Ariel Perez-Rosado, Alex Edgerton, Benjamin M Levi, Zeynep N Karakas, Mark Kujawski, Alyssa Philipps, Nicholas Papavizas, Danielle Fallon, Hugh A Bruck, and Elisabeth Smela. New compliant strain gauges for self-sensing dynamic deformation of flapping wings on miniature air vehicles. *Smart Materials and Structures*, 22(8):085031, 2013. doi:10.1088/0964-1726/22/8/085031.

[58] M. Kujawski, J.D. Pearse, and E. Smela. Elastomers filled with exfoliated graphite as compliant electrodes. *Carbon*, 48(9):2409 – 2417, 2010. doi:10.1016/j.carbon.2010.02.040.

[59] Cathy A. Fleischer, Jeffrey T. Koberstein, V. Krukonis, and P. A. Wetmore. The effect of end groups on thermodynamics of immiscible polymer blends. 1. interfacial tension. *Macromolecules*, 26(16):4172–4178, 1993. doi:10.1021/ma00068a016.

[60] Leszek A Utracki. *Polymer blends handbook*. Springer, 2003.

[61] C.M. Roland. Immiscible rubber blends. In P. M. Visakh, Sabu Thomas, Arup K. Chandra, and Aji. P. Mathew, editors, *Advances in Elastomers I*, volume 11 of *Advanced Structured Materials*, pages 167–181. Springer Berlin Heidelberg, 2013. doi:10.1007/978-3-642-20925-3_6.

[62] Manoj K Chaudhury. Rate-dependent fracture at adhesive interface. *The Journal of Physical Chemistry B*, 103(31):6562–6566, 1999. doi:10.1021/jp9906482.

[63] Cormac Flynn, Andrew Taberner, and Poul Nielsen. Mechanical characterisation of in vivo human skin using a 3d force-sensitive micro-robot and finite element analysis. *Biomechanics and modeling in mechanobiology*, 10(1):27–38, 2011. doi:10.1007/s10237-010-0216-8.

[64] Rachel B. Groves, Sion A. Coulman, James C. Birchall, and Sam L. Evans. An anisotropic, hyperelastic model for skin: Experimental measurements, finite element modelling and identification of parameters for human and murine skin. *Journal of the Mechanical Behavior of Biomedical Materials*, 18(0):167 – 180, 2013. doi:10.1016/j.jmbbm.2012.10.021.

[65] Yigit Menguc, Yong-Lae Park, Ernesto Martinez-Villalpando, Patrick Aubin, Miriam Zisook, Leia Stirling, Robert J Wood, and Conor J Walsh. Soft wearable motion sensing suit for lower limb biomechanics measurements. In *Robotics and Automation (ICRA), 2013 IEEE International Conference on*, pages 5309–5316. IEEE, 2013. doi:10.1109/ICRA.2013.6631337.

[66] Hiroyuki Shinoda and Hideki Oasa. Passive wireless sensing element for sensitive skin. In *Intelligent Robots and Systems, 2000.(IROS 2000). Proceedings. 2000 IEEE/RSJ International Conference on*, volume 2, pages 1516–1521. IEEE, 2000. doi:10.1109/IROS.2000.893235.

[67] Mitsuhiro Hakozaki and Hiroyuki Shinoda. Digital tactile sensing elements communicating through conductive skin layers. In *Robotics and Automation, 2002. Proceedings. ICRA'02. IEEE International Conference on*, volume 4, pages 3813–3817. IEEE, 2002. doi:10.1109/ROBOT.2002.1014314.

[68] Matthew A Nurse and Benno M Nigg. Quantifying a relationship between tactile and vibration sensitivity of the human foot with plantar pressure distributions during gait. *Clinical Biomechanics*, 14(9):667–672, 1999. doi:10.1016/S0268-0033(99)00020-0.

[69] Dortha Esch. *Evaluation of joint motion: methods of measurement and recording*. U of Minnesota Press, 1974.

[70] Meital Segev-Bar and Hossam Haick. Flexible sensors based on nanoparticles. *ACS Nano*, 7(10):8366–8378, 2013. doi:10.1021/nn402728g.

[71] Roger M Enoka. *Neuromechanical basis of kinesiology*. Human Kinetics Champaign, IL, 1994.

[72] Meng Yee Chuah, M. Estrada, and Sangbae Kim. Composite force sensing foot utilizing volumetric displacement of a hyperelastic polymer. In *Intelligent Robots and Systems (IROS), 2012 IEEE/RSJ International Conference on*, pages 1963–1969, Oct 2012. doi:10.1109/IROS.2012.6386239.